IMPROVING SOYBEAN USING REMOTE SENSING, AUTOMATED IRRIGATION, AND PROMISCUOUS NODULATION

BY

NATHAN EVAN SCHMITZ

THESIS

Submitted in partial fulfillment of the requirements
for the degree of Master of Science in Crop Sciences
in the Graduate College of the
University of Illinois at Urbana-Champaign, 2017

Urbana, Illinois

Adviser:

Professor Brian Diers

ABSTRACTS

Remote Sensing of Soybean Maturity Dates via Drones

High-throughput phenotyping (HTP) using remote sensing is a fast developing technology, which has the capacity to reduce the time it takes to measure phenotypic traits in the field. HTP shows particular promise as a method for predicting plant maturity. Maturity is the date where 95% of the pods reached mature color (R8 growth stage) and is commonly recorded on all yield plots in breeding programs by periodically walking through experiments and visually estimating maturity dates. Precise maturity dating is a time critical task; therefore, satellites and other previously developed methods of remote sensing would not be applicable to this research. To combat the limitations of other methods of remote sensing, we constructed a two-camera mounted Unmanned Aerial Vehicle (UAV) platform with the capacity to capture visible and near-infrared (NIR) images. This study was done in three broad steps: the acquisition of multi-spectral images using UAVs, constructing composite images of the visible and (NIR) images, and extracting digital values to build a model to predict maturity dates from images. Using these procedures, we were able to develop a binary prediction model from the multi-spectral image data and achieved over 91% accuracy in classifying soybean maturity. The maturity model was validated in an independent breeding trial with a different plot type. These results show that remote sensing can be effectively used to estimate the maturity of plots, but the analysis of images needs to be more efficient before it can be used routinely.

Automated Greenhouse SCN Screening System

Heterodera glycine (Ichinohe 1952) or soybean cyst nematode (SCN) is a pest of economic importance to soybean (*Glycine max* (L.) Merr.) in the USA and around the world.

From 2003-2009, SCN was estimated to reduce soybean yields more than any other disease or pest in the U.S.A. Methods of control include crop rotation and nematicides, but the most effective form of control is the use of resistant soybean cultivars. The current, established greenhouse screening method uses soil-filled crocks suspended in thermoregulated water baths to control the soil temperature. No current screening method controls the soil moisture to maintain optimal levels for SCN survival and propagation. With the use of soil moisture probes that automatically controlled an irrigation system, we were able to maintain the moisture levels at a constant level. Reproduction of the SCN was improved, with a significant increase in the number of cysts counted on the soybean roots. Overall, these results demonstrate that maintaining soil moisture increases the effectiveness of greenhouse screening methods for SCN.

Promiscuous Nodulation

Soybean (*Glycine max.*) is an important source of oil and protein for the U.S.A. and has the potential to be a staple crop in Africa because of its high protein seed and the benefits of nitrogen fixation from the symbiotic relationship with rhizobium bacteria. Soybean has a natural relationship with *Bradyrhizobium japonicum*, which is not indigenous to the tropical soils in Africa. For soybean to fix nitrogen with *B. japonicum*, inoculants of this bacteria would be needed, which are generally not available to small-holder African farmers. The cowpea strain of rhizobium bacteria is indigenous to the soils throughout Africa, although it does not nodulate most US soybean cultivars. Some soybean accessions from the USDA Soybean Germplasm Collection can nodulate with the cowpea strain and these are called promiscuous nodulators. The objective of this study was to identify additional accessions from the germplasm collection that are promiscuous nodulators. By screening plants in inoculated pots in a greenhouse, 415

accessions were evaluated for their ability to nodulate and if the nodules were effective. Of the lines tested, 200 were able to form effective, nodules and 42 lines showed no foliar signs of chlorosis due to nitrogen deficiency. Accessions that stood out were PI 429330 (Nigeria) for the highest number of nodules produced, and PI 281883C (Indonesia) for the one of the highest average nodule weights.

ACKNOWLEDGEMENTS

I would like to thank Dr. Brian Diers for providing this opportunity to conduct research under his helpful guidance and for his support and advice on my academic pursuits. I would also like to thank Chong “Neil” Yu for all his knowledge and advice on remote sensing.

Many thanks and gratitude goes to Troy Cary, Jake Tammen, and the rest of the farm crew for all their help and their technical knowledge. I would also like to thank lab technician Sarah Schultz, Lillian Brzostowski, Russell Ward, and countless undergraduates who aided with multiple aspects of research.

Finally, I would like to thank my family and friends for all their support throughout my academic career.

TABLE OF CONTENTS

CHAPTER 1

Remote Sensing to Predict Soybean Maturity Dates via Drones

Introduction

There have been many applications of remote sensing in agriculture. For example, aircraft have been used since the late 1920's to aid in U.S. soil surveys. Technology has since improved vastly in aiding agricultural professionals with the unique challenges they are presented. Current examples of the use of remote sensing include the estimation of yield (NASA 1977; Doraiswamy et al., 2003; Prasad et al., 2006), crop stress (Ustin et al., 1998), and environmental problems (Song et al., 2010).

First proposed in 1960 by the National Research Council, the Large Area Crop Inventory Experiment (LACIE) was an experiment aimed at developing a method for estimating production of the wheat crop worldwide. This did not become feasible though until the launch of the Landsat satellite on July 23, 1972, which allowed large scale remote sensing of wheat production to become reality, thus it became the first U.S. government sponsored program aimed at examining the feasibility of using remotely sensed satellite data to estimate wheat production over large areas (Nellis et al., 2009). Prior to LACIE, these estimations relied heavily on statistics and reports released by foreign countries (Erickson, 1984). The program was intended to establish an efficient analysis of the Landsat satellite and meteorological data in a timely and accurate manner and to create an estimate of global wheat production within 10% of the true estimate 90% of the time (NASA, 1977), referred to as the 90/90 criterion. The LACIE experiment became a joint operation comprised of the National Aeronautics and Space Administration (NASA), the US Department of Agriculture (USDA), and the National Oceanic and Atmospheric Administration (NOAA) (NASA, 1977; Erickson, 1984).

The LACIE experiment monitored three areas of major wheat production: the United States Great Plains, regions of Canada, and regions of the USSR (NASA, 1977). The basic approach of this experiment was to use land area planted, derived from Landsat data, and weather data, acquired from the World Meteorological Organization (WMO), to produce a model for wheat production in that area (Erickson, 1984). This approach found much success in the areas monitored in the Soviet Union. In August of 1977, the LACIE experiment produced its first accurate estimate for wheat, a spring wheat crop in the Soviet Union. The LACIE experiment's initial early estimate proved to be off by only six percent, while their final estimate was off by about one percent of the actual figure released by the USSR (NASA, 1977). Predictions were less successful in Canada, because of their different agricultural practices in growing wheat. At the time, Canada field size was generally smaller than that of the USSR and these smaller fields were at the resolution limits of Landsat 1. Canada also grew more crops that appeared similar to wheat from the data acquired from the Landsat satellite. Both issues led to inaccurate estimates of the land area planted for Canadian wheat production (Erickson, 1984).

Despite these limitations, the LACIE experiment showed that crop production estimations could be successfully made with satellites. In the 1980's, a follow up program, Agriculture and Resources Inventory Surveys through Aerospace Remote Sensing (AgRISTARS), continued the work of its predecessor. Both the LACIE and AgRISTARS programs developed methods for regional crop identification, condition assessment, and defined the physics of the relation between spectral measurement and biophysical properties of crop canopies and soils, and these methods are still in use today (Moran et al., 1997). According to Bailey and Boryan (2014), "These programs were successful at generating unbiased statistical

estimates of crop area at the state and county level and more importantly reducing the statistical variance of acreage indications from farmer reported surveys".

For remote sensing in agriculture, Vegetative Indices (VI) often play a role in evaluating, simplifying, and putting data into decipherable forms. These VIs vary on what they monitor or evaluate from the crop/field conditions. The Normalized Difference Vegetation Index (NDVI), Normalized Difference Water Index (NDWI), Leaf Area Index (LAI), and Vegetation Condition Index (VCI) are some examples of widely used indices.

Of the VIs used, NDVI tends to be the most popular of these indices (Gao, 1996). Studies using NDVI have demonstrated its ability to measure crop canopy chlorophyll content (Rulinda et al., 2011), detect early drought conditions (Song et al., 2010), and estimate crop yield (Doraiswamy et al., 2003; Prasad et al., 2006). The popularity of NDVI stems from its close relationship with canopy Leaf Area Index (LAI) and fraction of Absorbed Photosynthetically Active Radiation (fAPAR) (Atzberger, 2013). "Due to its almost linear relation with fAPAR, the NDVI can be readily used as an indirect measure of primary productivity" (Atzberger, 2013). Biophysical variables, (physical variations that can be observed in the plant ranging from plant structure to chlorophyll content), combined with NDVI can be used as an indirect measurement of plant maturity. Chlorophyll content, for example, has been related to the growth stage, photosynthetic activity, and plant stresses (Ustin et al., 1998).

Advances in low cost, high-throughput genotyping has rapidly increased the rate of genetic improvements and breeding efficiency (Jannink et al., 2010, Li et al., 2014, Montes et al., 2011). In contrast, high-throughput phenotyping has seriously lagged genotyping capacity (Araus and Cairns, 2014; Liebisch et al., 2015). The current typical approach to phenotyping is for an expert to visually evaluate plants or plots. There has been more demand recently for quicker and

more effective ways of phenotyping to keep pace with and support the improvements in genotyping.

Liebisch et al. (2015) recently produced a pipeline for phenotyping maize traits via aerial remote sensing. Multi-spectral images were taken regularly throughout the growing season to extract parameter values that correlated with ground measurements with the intent to identify phenological traits and morphological characteristics. They were able to show that it is possible to phenotype traits via aerial remote sensing at full canopy cover. For this, two row plots had higher reliability than one row plots. The study also demonstrated the timeliness of aerial remote sensing compared to that of ground-based methods (e.g. tractor mounted sensors).

Meng et al. (2013) was able to successfully predict the optimal harvest time for soybean through regression analysis of variations of NDVI and NDWI using imagery from the HJ-1 satellite constellation system belonging to China. This experiment looked to reduce the problems of within-field spatial variation that previous meteorological based regression models did not account for, with the overall objective to develop a model that led to optimal harvest yields and efficient use of time.

The two indices used in the Meng et al. (2013) study were significantly associated with harvest date, and the coefficients of determination were 0.403 and 0.595 for NDVI and NDWI respectively. The Root Mean Square Errors were 1.23 and 1.26 days. This study resulted in predictions of the optimal harvest date to within one day with over a 50% success rate, and within three days with over a 90% success rate. While the experiment proved to be successful, the author expressed the need to have a more accurate prediction model implemented for multi-temporal image analysis. With UAVs being able to capture multi-spectral images in a timely, daily manner, they are a reasonable choice for capturing images.

Zhang et al. (2014) performed a case study to look into the application of commercial UAV's to monitor crop conditions in a field through remote sensing. The team was able to construct NDVI mosaics of the fields using images collected with optical (visible) and NIR (Near Infrared) cameras. When they monitored a study in a farmer owned field that had different fertilizer treatments in soybean, they were able to identify which treatments had more positive effects on plant growth and yield. Also detectable by the UAVs was armyworm damage in wheat, although a severe storm caused lodging just prior to surveillance of the field.

Zhang et al. (2014) discussed factors that may be challenges for commercial use of the UAVs for producers and researchers. First being the cost of equipment used. While Zhang used more expensive LARS (Low Altitude Recon System), which can range from 20,000 – 70,000 USD, there are many low cost commercial units available today. Commercial units may lack some of the ability of the LARS, but they are capable of completing flight missions given appropriate weather conditions. Cameras used for the capture of visible and NIR images are also expensive and can cost upwards of 7,000 USD. In addition, the time required to process images to make mosaics can be an additional 3 hours of work, on top of the time needed to acquire images from the field.

Rating the maturity date of soybean experimental lines and cultivars is very labor and time intensive for breeders. The current method used to rate maturity dates is to visually check each plot at least weekly until all plots are mature. Plots are typically rated as mature when 95% of the pods on the plants in plots reach their mature color (Fehr et al., 1971). It is common for private industry breeding programs to have tens of thousands of plots that need to be evaluated each growing season, and the repeated trips through fields to record plant maturity requires a

large amount of time. Reducing the amount of time required to record these maturity dates would free time for other activities during the busy fall season.

With the use of satellites, remote sensing was shown to correctly detect soybean maturity to determine optimal harvest dates (Meng et al., 2013). Satellites show much promise in agricultural remote sensing and have been widely used because of the availability of the data, but due to the delay between the satellite passing over the same area and the chance of atmospheric/weather conditions affecting image quality, it would be hard to implement its use for something that is time critical such as soybean maturity dating. Other options such as aerial imagery via aircraft would be too costly to be effectively used in small programs or those with fields in multiple locations.

In the FAA reauthorization bill signed in 2012, the FAA and the Unmanned Aircraft Systems (UAS) industry were required to work together to develop a comprehensive plan that would fully integrate UAVs into the regulatory framework (Watts et al., 2012). This eventually lead to new policies being put in place in 2016 for commercial use of UAVs that includes laws dictating how drones can be flown and the requirement of a remote pilot certificate. UAVs provide the unique ability to survey crops daily or even multiple times a day, weather conditions permitting. Other promising characteristics are the long flight duration, improved mission safety, flight repeatability due to improving autopilots, and reduced operational costs when compared to manned aircraft (Watts et al., 2012).

A UAV was chosen for my study over the more extensively used satellites because UAVs have many advantages for image acquisition. Satellites have a set orbit, making time critical studies impractical, also resolution of the cameras may not be sufficient to capture the detail needed for predictions of small plots, and the images will not always be (near) vertical captures

of the object of interest (importance addressed below). Weather plays a factor in image quality for both satellites and UAVs as weather may be a hindrance to flight performance of UAVs, effectively grounding them. However, due to the flexibility of the UAV planning, flights during days with optimal weather are easily achievable. The biggest problem facing UAVs is the weight limit of each platform. Yet, it is possible to fix two cameras for multispectral analysis on many inexpensive platforms. For these reasons, in this study a UAV was chosen to develop a High Throughput Phenotyping Platform (HTTP) that would gather remote sensing data and with the use of machine learning, train a random forest model that will be able to accurately predict the maturity of soybean in a timely manner. The random forest model is a form of machine learning, used as regression model in this study.

Materials and Methods

The research plan can be split into three activities: acquisition of the remote sensing imagery, image processing, and extraction of data that are analyzed to make maturity predictions. All images were taken at a field located at the University of Illinois Crop Science Research and Education Center in Urbana, IL. The soybean plots used in the study were 6,400 plant rows of experimental lines derived from 106 different parental crosses from Dr. Brian Diers' breeding program at the University of Illinois and five checks (IA2102, LD02-4485, IA3023, IA3048, and LD06-7620). All the plant rows were 1-meter long single row plots with a row spacing of 0.76 meters. The plots were planted on 6/9/2014, and the plant row plots were not replicated. All ground truth data of maturity ratings were gathered by Dr. Diers' group by visual estimates. Soybean plants were considered fully mature at the R8 growth stage, defined as 95% of the pods on the plants having turned to their mature color. Visual estimates were taken 3-4 days apart.

Image Acquisition

Multi-spectral images used in the study were collected with a UAV that was purchased from 3D Robotics (San Diego, California). The UAV purchased is the model X8 octocopter, which was chosen for its low cost, easy "Ready to Fly" package, and its ability to autonomously fly with set GPS coordinates.

To capture images, cameras that capture visual and near-infrared light were mounted on the UAV facing directly down. Visible and NIR light was used due to the strong contrast between these wavelengths for reflectance from vegetation. Two Cannon PowerShot S110 12 MP Digital Cameras equipped with complementary metal-oxide semiconductor sensors were used. To capture the near-infrared images, one camera was sent to Kolari Vision (Raritan, New Jersey), which made modifications to the camera by installing a 720 nm long pass filter.

To continuously capture images when the UAV was flying, the cameras were programed with a script to capture an image every second. To cover the entire field, the UAV was programmed using the Mission Planner ground station software to fly a scripted route using GPS. Overlap of the images taken was 80% forward overlap and 60% side overlap. Options available in the Mission Planner software allowed for computer generated flight plans that account for image capture delay and then adjustments in the flight speed and route were made to produce a flight plan with the desired amount of overlap. The script produced had the UAV flying at 6 m sec^{-1} at an altitude of 95 m. The images produced have a coverage footprint of approximately 138.8-by-104.1 m, and the spatial resolution was 3.47 cm/pixel. The UAV was flown on multiple dates so that maturity predictions could be made across the time that the plots matured. The images were captured on 7/24, 8/25, 9/4, 9/19, 9/23, 9/26, 9/30, 10/6, 10/20. The large gap between the final two image dates was due to unfavorable weather conditions and crew

unavailability because of the priority of harvest. Multiple dates of image capture were needed for accurate model building and maturity prediction.

Image Processing

Each image was selected based on quality before being used. Quality selection was done by both visual checks and software analysis. Images that were blurry or did not capture areas of interest were discarded. Image quality was also determined using the quality score, which is a software measurement of the image sharpness, given by the image software Photoscan Pro, and images with a quality score less than 0.6 were discarded.

The individual images were combined into orthophotos for data extraction. Permanent place markers, or ground control points (GCP), were located throughout the field and served as landmarks for stitching together images (Figure 1.1). These GCPs were plywood boards, roughly 0.5 meter by 0.5 meter, painted white with a black cross through the center. The GCPs were mounted onto metal poles approximately a meter from the ground. The GPS coordinates of the GCPs were taken using a survey grade Trimble GPS unit (Trimble Navigation, Ltd, Sunnyvale, California). These coordinates were used to geo-reference the orthophotos. A calibration board was also placed in the field and used as a place marker. The calibration board was roughly 1 meter by 1 meter, with a checkered pattern of 2 black and 2 white blocks. In addition to being used as place markers, the calibration boards were used in the normalization of the digital values extracted from the images.

Using the stitching software Agisoft PhotoScan Professional (Agisoft LLC, St. Petersburg, Russia), the multiple images were combined into visible light and NIR orthophotos of the field. The GCPs uploaded with the GPS coordinates were manually identified in each image. This allowed the software to use the GCPs as reference points to combine the images. For

orthophoto construction, “Interpolation” mode in the “Build Mesh” stage was disabled. This caused the software to only use available points in the dense point cloud. “Mosaic” was set to “Blending mode”. During the texture generation process, this caused the software to only use pixels the shortest distance from the center of the image. This disables the software from overlapping the photos, or averaging them, improving the accuracy of the pixel values used. In the end, a geo-referenced orthophoto for visible light and a second for NIR were produced. The orthophotos were exported as Geo-TIFF format and later imported to GIS software, ArcGIS. In ArcGIS, the visible light and NIR orthophotos were used to generate a composite multispectral image. Each orthophoto was comprised of 3 bands, a Blue-channel, a Green-channel, a Red-channel. Only the Blue-channel from the NIR image was used in the formation of the composite. This was due to concern over the potential that the Red-channel would be contaminated with visible light.

Further refinement of the NIR/Visual light composite image was needed. The areas of interest (individual plots) were clipped out of the whole image, producing rectangular clippings of just the plant row blocks of interest. The number of rows and columns of the plant rows in the clipped block were noted for later use.

Data Extraction and Model Building

The remainder of the analysis was completed with the software program RStudio (The R Foundation for Statistical Computing 2015, version 3.2.2). Using regression models and machine learning, the reflectance data were used to predict soybean plant maturity. The reflectance data used in the analysis were the pixel values, or Digital Numbers (DN), which measure the reflectance given off by plants. These DNs needed to be normalized for each date images were taken before they could be used in model building. The calibration board described

earlier was used as a standard form of light reflectance to normalize the DN of the remaining pixels in the images.

The reflectance values of the four bands that comprise the composite photos have a linear relationship with the DNs. The images from the different dates were normalized using the following equation:

$$Black_{T1,k} = a_k \times Black_{T2,k} + b_k$$

$$White_{T1,k} = a_k \times White_{T2,k} + b_k$$

where $Black_{T1,k}$, $Black_{T2,k}$ (dark reference), $White_{T1,k}$, $White_{T2,k}$ (bright reference) are the DNs of the band (k) of the image taken from time one ($T1$) and time two ($T2$) and a_k is the slope and b_k is the intercept (Hall et al., 1991, Yang and Lo, 2000). The DN of the dark reference object was extracted and averaged from 60 geo-stationary pixels at the black part of the calibration board for given bands of the multispectral image. The DN values were for the bright reference also originally to be extracted from the calibration board, but due to overexposure, the bright reference needed to be taken from another reference object. The new reference object chosen was a light grey shed next to the field. Due to it being not completely white, it was not oversaturated in the images. The image used as a reference image, "T1", was taken on September 19, 2014. Subsequent normalization coefficients of images were calculated using the previously given equation and applied to the whole image to accomplish the radiometric normalization.

Using the row and column number from each clipping, the plant row studies were broken down into their individual plots. In ArcGIS, the "Fishnet" function was used on the clippings to visually check that the plots contained the plant rows. From there, the normalized pixels were extracted for use in model building. Pixels were extracted two different ways to build two different models and to test if one was superior. First, pixels were extracted from the whole plot.

This included the whole row of plants and soil that was not covered by foliage. Potential problems that could arise from this method are that the soil from the image may skew the model and/or produce an invalid prediction. The second method used only the center three rows of pixels from each plot. Using only the center three rows reduced the amount of non-foliage pixels in model building and prediction analysis.

The DNs of the plots were averaged and associated with ground truth data of plot maturity. The ground truth data for each date and plot were labeled either as being "Mature" or "Non-Mature" at the time of the image capture. A random forest model was developed, using the R package 'randomForestSRC' (Ishwaran, 2015). The plant rows were divided into two even groups. Half were used to train the random forest model, using the DNs and the ground truth labeling. The second group was used to validate the effectiveness of the model to predict maturity. The predicted maturity dates produced by the random forest model were then compared to the ground truth data to calculate accuracy.

Time Allocations

Time inputs for this project varied by the step, and all time estimates below are for each day of image capture. Acquiring images is done during the summer and fall, but only requires one to two hours every four days starting from when the plants began to set pods until harvest. Image quality screening takes roughly an hour. Image processing can take up to three hours per image produced, and this time varies based on the processing speed of the computer used. Overall, the process can take 4-6 hours for each image; however, the actual time that a person needed to be present is roughly half this time.

Extracting the data using the GIS software ArcGIS is tedious because someone has to be physically present throughout the process to insure optimum data accuracy. Current methods

require a person to clip segments of the field being studied which requires an hour of work for each composite image. After this, analysis in the statistical software R studio was used in the prediction model. The final step of extracting data from plots in one full composite image (6,800 single row plots) takes upwards of eight hours; however, the actual input of human time is minimal. It took approximately 15-30 minutes to rewrite the code for each composite image and to insure that the script ran correctly.

From start to finish, this process can take longer than 10 hours. The actual time that a human needed to be present was roughly 4-5 hours for each date the images were taken.

Results

The experimental plant rows used in this study were being developed as potential new cultivars for Illinois. They ranged in maturity from early maturity group (MG) II to late MG IV. Image quality was crucial to producing an accurate prediction model. Not all images were of sufficient quality and if possible, these poor quality images were not used in making composite images. When images were discarded, this potentially could leave gaps if many images in a row were of poor quality, and this led to a few blurred areas in some of the composite images. The main cause of blurriness was high wind and because of this, low wind was often the deciding factor on when to fly. This led to an increase of the quality of images captured. The use of a gyroscope or other free moving device to stabilize the cameras would aid in image quality; however, a gyroscope could not be used in this study because of the weight limits of the UAV used.

Data collected in the experiment were analyzed with the random forest model using two different pixel extraction methods. The first method used pixels from the whole plots and the second used the center three columns of pixels from each plot. Each of these methods were used

to build separate models using one half of the plot data and then tested on the other half. The accuracy of the maturity predictions for these two methods was similar (Figure1.2 and 1.3). The overall maturity prediction accuracy (the accuracy of the random forest model to correctly predict whether a plot was mature or not-mature on a given date compared to the ground truths) was approximately 91%. The kappa coefficient, which controls for correct predictions that result from random chance, was 66%. This demonstrates that there was good agreement between the ground truth maturity estimates and the random forest model predictions, and they did not just match due to chance. Though a high overall accuracy was observed, there was difficulty in detecting the mature plots. Of the mature plot predictions, 75% were accurately estimated on the exact date of maturity. The remaining 25% were predicted to be mature early, when compared to the visual ground truths (Figure 1.2, Confusion Matrix). Vice versa, 33% of the mature plots according to the ground truth data were not predicted as mature on the visually estimated date.

In a previous study, Yu et al. (2016) trained a random forest model for maturity prediction using different source material that was grown in the same field as the current study. In the Yu et al. (2016) study, the model achieved a 93% overall accuracy when tested on plots in the same study that was used to train it. The Yu et al. (2016) model was then tested on the germplasm in the current study, which resulted in a slight decrease in accuracy to 91% for the analysis with both whole plots and center plot pixels (Figure 1.4 and 1.5). This shows that the maturity prediction models can be successfully applied to studies in which they were not developed.

The number of days to maturity predictions differed from the manually taken maturity notes is shown on Figure 1.6. As expected, the model trained with data from the current study had a higher percentage of correct predictions of the exact maturity date with a 77% accuracy

compared to predictions with Yu's model that had a 49% accuracy. The model trained in the current study was able to predict maturity 91% of the time within +/-1 date (a date being a day when data was taken with the UAV, there were typically 3-4 days between these dates). Yu's model had a similar success rate and was able to predict maturity 92% of the time within +/-1 date.

Discussion

The random forest model was able to accurately predict the maturity of soybeans with 91% overall accuracy using both the model from Yu et al. (2016) and the model developed in the current study. The use of whole plot or center column of pixels had similar success in predicting soybean maturity, which suggests that soil captured in the images and other interferences did not affect the maturity prediction. Inaccuracies in predicting soybean maturity at least partially stems from how maturity is determined. Soybean maturity is based on pods losing their chlorophyll and this does not necessarily align with leaf chlorophyll loss and senescence, which is what is largely detected by the images taken by the UAV. Predictions are especially difficult when green stem disorder is present in the field or when green leaves still remain on a fully mature plant. Green stem disorder can result in plants reaching R8, with 95% of the pods turning to their mature pod color, but with plants retaining green leaves and stems (Hill et al., 2006). The random forest model could view the greenness as not a mature plant, resulting in an incorrect prediction.

The traditional method of estimating maturity done by walking through the field and manually dating when plots are going to be mature is also error prone. Within the Diers lab there were eight different people taking maturity notes during 2014, resulting in minor differences in maturity ratings depending on who rated the plots. Allowing the random forest to have an

acceptable amount of error, plus or minus one date, raises the accuracy of determining mature plots to 92% and 91% for the previous and new model, respectively (Figure 1.6).

While the model developed in the current study had a higher exact maturity prediction compared to Yu's model (Figure 1.6), Yu's model maintained a slightly higher accuracy when an error of plus or minus one date was allowed. It was expected that the new model would be better at predicting the exact date of maturity as it was trained using the same material was it was tested. Both models were developed using plant rows from the breeding program, but the material used to develop Yu's model had a wider range in maturity when compared to the newer model's source material. It is possible that this wider range in maturity resulted in Yu's model performing better than the model developed in the current study; however, additional research is needed to verify this theory.

The main goal of this project was to set up a high throughput phenotyping pipeline that could be used to predict soybean maturity in a timely manner. The models developed were largely successful in predicting maturity, and the images from a single date can be processed in less than 10 hours, with only half the time human presence needed. This is less than the amount of time required to take manual notes in the field; however, improvements in the analysis pipeline could reduce the amount of time needed to predict maturity much further and would make high throughput phenotyping for predicting maturity a reality for soybean breeders.

Figures

Figure 1.1. A. One of multiple place markers in the field that served as a permanent geo-referenced marker used in composite image formation. B. Calibration board, used for radiometric normalization of images, also served as geo-referenced place marker. C. A single, visual light image with place markers circled to show the presence of multiple place markers in images. D. A composite image containing both visual and NIR bands with place markers and calibration board circled.

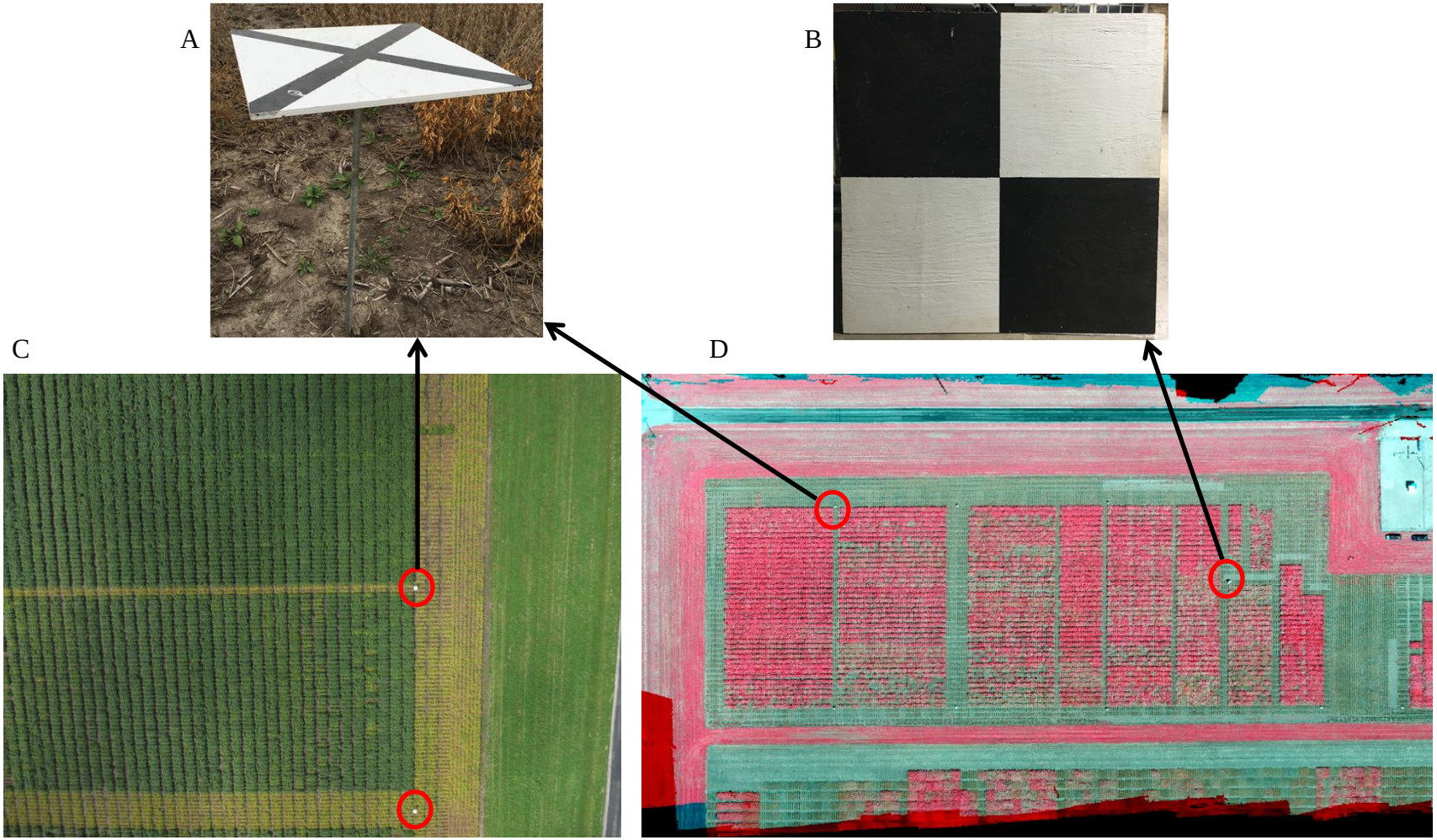

Figure 1.2. Confusion matrix and statistics for maturities predicted using a random forest model developed in the current study and run with the pixels from whole soybean plots. Observed axis includes ground truth visual maturity recordings, predicted axis are maturity predictions from the random forest model.

Confusion Matrix

Predicted \ Observed	Yes	No
Yes	1518	500
No	758	13198

Accuracy Statistics

Terms	Value
Accuracy	0.9197
Accuracy 95% CI	(0.9154, 0.9239)
Sensitivity	0.65914
Specificity	0.96350
"Yes" Pred Value	0.75223
"No" Pred Value	0.94386
Prevalence	0.14393
Kappa	0.6564
Balanced Accuracy	0.81132

*Accuracy was referred to as overall accuracy in results

Figure 1.3. Confusion matrix and statistics for maturities predicted using a random forest model developed in the current study and run with the pixels from the three center columns from each soybean plot. Observed axis is ground truth visual maturity recordings, predicted axis is the random forest model's predictions.

Confusion Matrix

Predicted \ Observed	Yes	No
Yes	1557	502
No	746	13196

Accuracy Statistics

Terms	Value
Accuracy	0.922
Accuracy 95% CI	(0.9177, 0.9261)
Sensitivity	0.67607
Specificity	0.96335
"Yes" Pred Value	0.75619
"No" Pred Value	0.94649
Prevalence	0.14393
Kappa	0.6689
Balanced Accuracy	0.81971

*Accuracy was referred to as overall accuracy in results

Figure 1.4. Confusion matrix and statistics for the random forest model previously trained (Neil's model) and run with the pixels from the whole soybean plot (Yu et al. 2016). Observed axis is ground truth visual maturity recordings, predicted axis is the random forest model's predictions.

Confusion Matrix

Predicted \ Observed	Yes	No
Yes	3104	1321
No	1501	26074

Accuracy Statistics

Terms	Value
Accuracy	0.9118
Accuracy 95% CI	(0.9087, 0.9149)
Sensitivity	0.6740
Specificity	0.9518
"Yes" Pred Value	0.7015
"No" Pred Value	0.9456
Prevalence	0.1439
Kappa	0.6362
Balanced Accuracy	0.8129

*Accuracy was referred to as overall accuracy in results

Figure 1.5. Confusion matrix and statistics for the random forest model previously trained (Neil's model) and run with the pixels from the three center columns from each soybean plot (Yu et al. 2016). Observed axis is ground truth visual maturity recordings, predicted axis is the random forest model's predictions.

Confusion Matrix

Predicted \ Observed	Yes	No
Yes	3247	1544
No	1544	25851

Accuracy Statistics

Terms	Value
Accuracy	0.9093
Accuracy 95% CI	(0.9061, 0.9124)
Sensitivity	0.7051
Specificity	0.9436
"Yes" Pred Value	0.6777
"No" Pred Value	0.9501
Prevalence	0.1439
Kappa	0.6380
Balanced Accuracy	0.8244

*Accuracy was referred to as overall accuracy in results

Figure 1.6. Comparison of predicted soybean maturities with ground truth maturities based on visual field observations for both the random forest model from Yu et al. (2016) and the new trained model from the current study. The data were analyzed using the pixels from the whole plot. Each "Date" is a day that the UAV was flown over the field, Dates were usually 3-4 days apart.

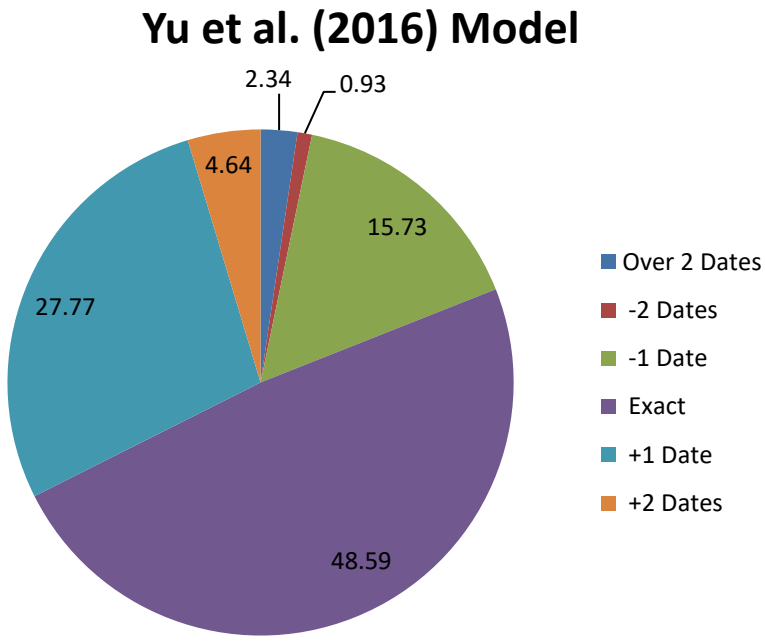

Accuracy within +/- one date, 92.09%

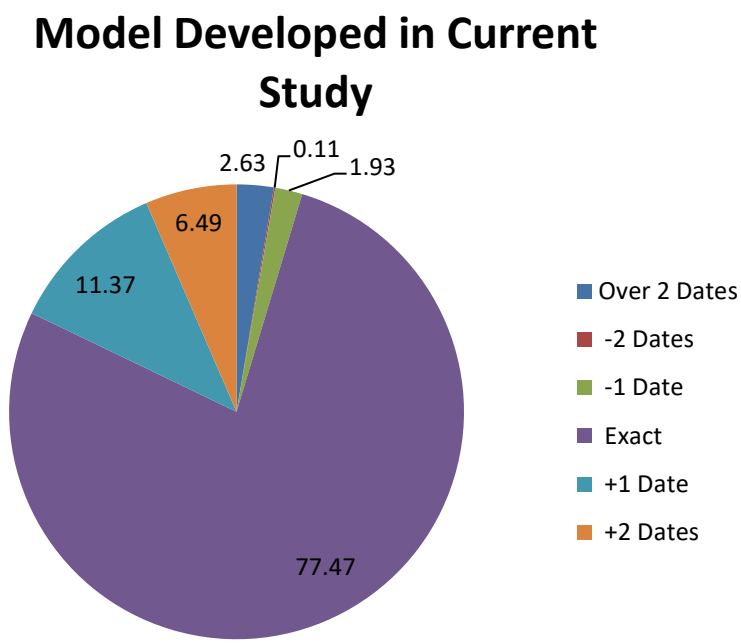

Accuracy within +/- one date, 90.77%

Literature Cited

Andrade-Sanchez, P., M.A. Gore, J.T. Heun, K.R. Thorp, A.E. Carmo-Silva, A.N. French, A.N. Salvucci, and J.W. White. 2014. Development and evaluation of a field-based high-throughput phenotyping platform. Functional Plant Biology. 41:68-79.

Araus, J.L., and J.E. Cairns. 2014. Field high-throughput phenotyping: The new crop breeding frontier. Trends in Plant Sci. 19:52-61.

Atzberger, C. 2013. Advances in remote sensing of agriculture: context description, existing operational monitoring systems and major information needs. Remote Sensing. 5:949-981.

Bailey, J.T., and C.G. Boryan. 2010. Remote sensing applications in agriculture at the USDA Nat. Agric. Statistics Service.

Berni, J.J., P.J. Zarco-Tejada, L. Suárez, and E. Fereres. 2009. Thermal and narrowband multispectral remote sensing for vegetation monitoring from an unmanned aerial vehicle. IEEE Trans. Geosci. Remote Sens. 47:722-738.

Doraiswamy, P.C., S. Moulin, P.W. Cook, and A. Stern. 2003. Crop yield assessment from remote sensing. Photogramm. Eng. Remote Sens. 665-674.

Erickson, J.D. 1984. The LACIE experiment in satellite aided monitoring of global crop production: Woodwell, George, The Role of Terrestrial Vegetation in the Global Carbon Cycle: Measurement by Remote Sensing. John Wiley & Sons Ltd. 191-217.

Fehr, W., C. Caviness, D. Burmood, and J.S. Pennington. 1971. Stage of development descriptions for soybeans, *Glycine max L*. Merrill. Crop Sci. 11:929-931.

Gao, B. 1996. NDWI - A Normalized Difference Water Index for remote sensing of vegetation liquid water from space. Remote Sens. Environ. 52:257-266.

Gardner, D.R. 1957. The national cooperative soil survey of the United States Ph.D. diss., Harvard University, Cambridge, Mass. Nat. Resources Conservation Service.

Hobbs, H. A., C. B. Hill, C.R. Grau, N.C. Koval, Y. Wang, W.L. Pedersen, L.L. Domier, and G. L. Hartman. 2006. Green stem disorder of soybean. Plant Dis. 90: 513-518.

Ishwaran, H., and U. Kogalur. 2015. Random forests for survival, regression and classification (RF-SRC). R package version 1 6 1.

Jannink, J., A.J. Lorenz, and H. Iwata. 2010. Genomic selection in plant breeding: From theory to practice. Briefings in Functional Genomics. 9:166-177.

LACIE Phase II Evaluation Report 1997 (LACIE-00453, JSC-11694). Houston, Texas.

Li, L., Q. Zhang, and D. Huang. 2014. A review of imaging techniques for plant phenotyping. Sensors. 14:20078-20111.

Liebisch, F., N. Kirchgessner, D. Schneider, A. Walter, and A. Hund. 2015. Remote, aerial phenotyping of maize traits with a mobile multi-sensor approach. Plant Method. 11:9.

Meng, J.H., T. Dong, M. Zhang, X. You, and B. Wu. 2013. Predicting optimal soybean harvesting dates with satellite data (J. V. Stafford, Ed.). Precision Agriculture. 209-215.

Montes, J., F. Technow, B. Dhillon, F. Mauch, and A. Melchinger. 2011. High-throughput non-destructive biomass determination during early plant development in maize under field conditions. Field Crops Res. 121:268-273.

Moran, M.S., Y. Inoue, and E.M. Barnes. 1997. Opportunities and limitations for image-based remote sensing in precision crop management. Remote Sens. Environ. 61:319-346.

Nellis, M.D., K.P. Price, and D. Rundquist. 2009. Remote sensing of cropland agriculture. The Sage Handbook of Remote Sensing.

Prasad, A.K., L. Chai, R.P. Singh, and M. Kafatos. 2006. Crop yield estimation model for Iowa using remote sensing and surface parameters. Int. J. of Applied Earth Observation and Geoinformation. 8:26-33.

Rulinda, C.M., W. Bijker, and A. Stein. 2011. The chlorophyll variability in Meteosat derived NDVI in a context of drought monitoring. Procedia Environ. Sci. 3:32-37.

Song, X., G. Saito, M. Kodama, and H. Sawada. 2010. Early detection system of drought in East Asia using NDVI from NOAA/AVHRR data. International J. of Remote Sensing. 25:3105-3111.

Ustin, S., M. Smith, S. Jacquemoud, M. Verstraete, and Y. Govaerts. 1998. GeoBotany: vegetation mapping for Earth sciences. Manual of Remote Sensing. 3:189-248.

Watts, A.C., V.G. Ambrosia, and E.A. Hinkley. 2012. Unmanned aircraft systems in remote sensing and scientific research: classification and considerations of use. Remote Sens. 4:1671-1692.

Yu, N., L. Li, , N. Schmitz, L.F. Tian, J.A. Greenberg, & B.W. Diers, (2016). Development of methods to improve soybean yield estimation and predict plant maturity with an unmanned aerial vehicle based platform. Remote Sensing of Environ. 187: 91-101. doi:10.1016/j.rse.2016.10.005

Zhang, C., D. Walters, and J.M. Kovacs. 2014. Applications of low altitude remote sensing in agriculture upon farmers' request- a case study in Northeastern Ontario, Canada. PLOS One. 9.

CHAPTER 2

Automated Greenhouse SCN Screening System

Introduction

Heterodera glycine (Ichinohe 1952) or soybean cyst nematode (SCN) is a pest of economic importance to soybean [*Glycine max* (L.) Merr.] in the U.S.A. and around the world (Zhang et al. 2016). SCN is a parasitic round worm that infects roots of soybean plants. The life cycle of the SCN can be broken down into three stages: egg, juvenile, and adult. The juvenile stage of the nematode actively seeks out host plant roots. The females will then remain stationary for the remainder of its life cycle and after mating will swell to form an egg sack with their body, called a cyst. At the optimal soil temperature of 25°C, the life cycle is approximately 21 days, with the development process slower at lower temperatures (Lauritis, 1983).

SCN was first observed in the USA in North Carolina in 1954, and by 1959 it was reported in Illinois, Arkansas, Mississippi, Missouri, Tennessee, and Virginia (Noel, 1993). It is now present in all major soybean-producing states in the USA and is recognized as one of the leading soybean pests (Koenning and Wrather, 2010). From 2003-2009, SCN was estimated to reduce soybean yields more than any other disease or pest in the USA (Wrather et al., 2006; Koenning and Wrather, 2010). SCN may reduce yields up to 30% in fields without showing any symptoms, such as reduced plant height or chlorosis (Niblack, 2005).

Forms of SCN control include crop rotation, resistant cultivars, and nematicides. Crop rotation is effective if the rotation leaves soybean and other host plants out of the rotation for 3-4 years. Unfortunately, the typical Midwestern rotation of growing soybean every other year does not prevent the establishment of SCN in fields (Noel, 1993). The efficacy of other control options such as nematicides has been inconsistent and treated susceptible cultivars typically have

lower yields than untreated resistant cultivars (Young, 1996). The most efficient way to control SCN is to plant resistant soybean cultivars in rotation with non-host crops (Arelli, 2000).

SCN populations were originally classified with a race system using soybean differentials. The system allowed for the classification of 16 different races (Riggs and Schmidt, 1988). The race system was later replaced with a *Heterodera glycine* type system to better differentiate SCN populations (Niblack et al., 2002).

In a study by Kopisch-Obuch and Diers (2005), segregation distortion was reported for the major SCN resistance gene *rhg1* in F_4 populations. They found that the number of plants homozygous for the *rhg1* resistance allele that emerged in the field was less than expected based on Mendelian segregation ratios. The authors speculated that the phenomenon was not caused by random genetic drift, but some form of selection at the *rhg*1 locus.

The *rhg*1 gene is responsible for the majority of resistance against SCN race 3 (HG type 0 or 7) and race 14 (HG type 1.3.7) from several resistance sources (Concibido et al., 2004). There have been five resistance genes identified in soybean through traditional genetics studies (*rhg1*-*rhg5*) (Concibido et al., 2004), and the *rhg*1-b allele, derived from the plant introduction (PI) 88788, is the most common commercially used SCN resistance gene (Kim et al., 2010).

Greenhouse screening is a reliable way to determine the SCN resistance of soybean genotypes. There have been studies to find the optimal soil temperature for the development and survival of SCN (Lauritis, 1983), and based these results, researchers have integrated the optimal temperature into thermo-regulated water baths used for SCN resistance evaluation (Niblack et al., 2002). Another major factor in determining the success of greenhouse screening for SCN resistance is soil moisture. Heatherly et al. (1982) studied the effects of soil water potential (SWP) in the upper 15 cm of soil on the development of cysts, and they found that the optimal

SWP was between -0.3 to -0.4 bars. Little work has been done, however, to develop methods to control soil moisture in greenhouse screens.

The objective for this study was to develop a method to improve the accuracy and consistency of results from SCN resistance screening with an automated watering system that uses a soil moisture probe to maintain optimal soil water levels. This system utilizes the greenhouse thermo-regulated water bath method outlined by Niblack et al. (2002). Watering rates are critical in greenhouse SCN studies as either too much or too little water will reduce SCN reproduction. Providing the correct amount of water is especially difficult in these tests because the plants are grown in crocks that are in a water bath and therefore have no drainage, resulting in waterlogging when too much water is applied.

Materials and Methods

Evaluations were done by growing plants in a temperature regulated water bath in a greenhouse (Niblack et al., 2002). The evaluations included the genotypes LD01-5907 and LD00-2817P (Diers et al., 2010), which have resistance tracing to PI 437654; LD00-3309 (Diers et al., 2006), which has resistance from PI 88788; and the susceptible cultivars Macon (Nickell, 1996), Lee 74 (Caviness et al., 1974), and IA3023. These genotypes and cultivars were germinated on germination paper 48 hours prior to the experiments being set up. The individual seedlings were transferred into plastic crocks fill with sterilized soil and partially submerged in the water bath. Each crock contained 23 PVC tubes that were each 16 cm high and 3 cm in diameter, with 22 containing soil and plants while one was empty and used for watering. The center, empty tube is filled with water everyday, allowing the water to percolate through the whole crook evenly. The soil in each tube was then inoculated with ~2000 SCN eggs of HG Type 0 and a germinated seedling was planted in each tube. The eggs were obtained from Alison Colgrove, a senior research specialist at the University of Illinois Urbana-Champaign. The plants

in tubes were arranged in an incomplete split plot design with automatic vs. manual watering being main plots and soybean genotypes and cultivars subplots. The main plots were replicated 4 times and genotypes and cultivars were replicated 3-4 times in each whole plot, giving either 14-15 total replications of a genotypes in both the manual and automated watering systems. Each crook was filled entirely, but this left unequal reps. Reasoning for this being it was unknown if having a crock partially filled would affect the moisture levels. The crocks were randomly placed in two rows in the water bath, so that it formed a 2x4 grid. The temperature of the water bath was set 27°C, and for the first week after planting, both the manual and automated systems were hand watered. At this stage, the root systems of the newly transplanted seedlings were not extensive enough to be watered by filling the center tube. Each PVC tube containing a plant was watered daily with approximately 5 mL of water.

For those crocks that were watered by hand (manual system), every morning the center PVC tube was watered at the same time (within 15 minutes of the hour). Hand watering worked by using a watering wand, or another narrow hose apparatus, and filling the center tube to the top. This allowed for each crook to receive approximately the same amount of water, with each PVC tube being capable of holding approximately 165 mL of water. For those crocks watered with the automatic system, the center watering tube had a drip emitter attached. The drip emitter system is part of a commercial garden watering system. The system is comprised of a pressure regulator [Senninger 3/4" FPT x 3/4" FPT Low Flow Regulator 12 PSI (Clermont, Florida)], a stainless steel filter [JAIN irrigation (Jalgaon, India)], 3/4” and 1/8” polyethylene tubing (Jain irrigation), pressure compensating emitters [Netafim (Hatzerim, Israel)], and flush valves (JAIN irrigation). In a tube that contained a plant, an EC-5 Decagon soil moisture probe (Pullman, WA) was placed in the soil, with the prongs reaching a depth of approximately 6 cm. This probe

transmitted data to the greenhouse software, Argus (Surrey, BC, Canada), which activated a solenoid valve releasing water to each crock for a set amount of time, which was calibrated to release approximately 15 mL. The moisture level set to trip the solenoid valve was 51% Volumetric Water Content (VWC), this value was determined using the default moisture level settings of the EC-5 Decagon. Due to the cost and practicality limitations, only two soil moisture probes were used, one for the automated watering system and the other for the manual. The soil moisture probe took soil moisture data at set time intervals for both the manual and automated watering systems for later comparison. The moisture probes took data every 15 seconds to determine if activation of the solenoid valve was needed.

After 28-30 days, the crocks were taken down, and the PVC tubes were soaked in water for 10 minutes prior to root extraction to reduce chances of root damage and dislodging of cysts from the roots. By pulling on plant stems, the roots were then removed from the tubes and rinsed under low water pressure to wash away soil. After removing as much loose material as possible, the roots were then placed in water filled 50 mL plastic tubes with caps. These were placed in a cold room until time allowed for the removal of the cysts.

For cyst extraction, a strong jet of water was used to dislodge the female cysts from the roots. The root mass was placed over a sieve with a 1 mm openings stacked onto a second sieve with a 250 micron openings (Fisher Scientific International, Inc., Pittsburg, PA). Female cysts were then counted under a light microscope, and the female index (FI), described by Niblack et al. (2002), was determined for each plant and used in the statistical analysis of the results. The formula for the FI is the average number of cyst on a tested line divided by the average number of cysts of the standard susceptible, with Lee 74 used as the standard susceptible line in this

study. If the value is higher than 0.1 (10 percent), the line is considered susceptible, or the SCN population is considered virulent and able to overcome resistance in the plant.

Results

The plants watered with the automated system had a significantly ($p < 0.0001$) greater number of females on their roots at the end of the experiment than plants manually watered (Table 2.1). This was largely due to the significant ($p < 0.0001$) increase of cysts forming on the susceptible cultivars (Lee 74, Macon, and IA3023) under the automated system compared to the manual system. The susceptible cultivars all had a significant increase in cyst number with the automated system, with a 185.5% ($P < 0.0001$), 62.5% ($P < 0.0001$), and 112.0% ($P < 0.0001$) increase for Lee 74, Macon, and IA3023, respectively. The three remaining tested lines, LD00-3309 (resistance), LD00-2817P (resistant), and LD01-5907 (resistant), showed no significant ($\alpha=0.05$) change in nematode number between the automated and manual watering systems compared to the manual watering system.

The female index (FI) values of the genotypes watered with the automated system were lower than those manually watered (Table 2.2). The decrease was largely due to the 185.5% increase of cyst counts on Lee 74, the denominator used in calculating the FI.

After the initial week of individual plant hand watering, both the manual and automated watering had fairly consistent moisture levels (Figure 2.1), the manual system took additional time to level out. The automated system had a smaller standard deviation (automated = 1.53, manual = 2.67) for moisture levels after individual plant hand watering was concluded. Along with the reduced variation in moisture levels, the automated system allowed for the ability to easily raise or lower the VWC to the desired level.

Discussion

Plants of the susceptible cultivars watered with the automated had large and significant increases in cyst number compared to the manually watered plants. This was especially true for Lee 74, which had an increase in cyst number from 132 for manual watering to 377 for automatic watering (Table 2.1). In contrast, no significant increases in cyst number was observed for the resistant genotypes. This resulted in lower FI values for the resistant genotypes. Lower FI values were also observed for the susceptible cultivars Macon and IA3023 as the result of the greater cyst increase for Lee 74 than for the other susceptible cultivars. These differences did not result in any changes in the resistant or susceptible ratings of the genotypes in the test.

Maintaining optimal moisture levels should improve SCN survivability and reproduction, leading to increases to cyst levels. Data collected from this experiment supports this theory. When watering of the center tube began (11/28, Figure 2.1) a benefit of the watering system is shown. Immediately after activation, the moisture level raised to the desired amount (51% VWC) and was maintained at this level consistently. After the initial week of hand watering each individual plant, the automated system leveled out to its specified VWC, the manual watering took a week to level out. This could indicate that this is a critical time (second week of study) for nematode development/survival, though additional research is needed to verify this. Early differences in the crock moisture levels were apparent before watering began, and this was most likely caused during set up. While inoculating the soil and transplanting, the soil is kept moist, but not saturated. The soil is moistened without measuring the water used which can lead to moisture variability within and among the crocks. Due to budget and design constraints in building the automated system used in this study, the automated watering was controlled by a single moisture probe in one crock; however, because the same number of plants were grown in

each crock, similar levels of transpiration was expected to occur in each crock, and the single moisture probe was able to control the entire system.

Ease of use was another justification for developing the automated watering system. While the automated system needs to be routinely checked for problems, the time regiment requirements are not as strict as the manual system. The manual system requires that the individual waters the plants at the same time daily. Failure to do so, even late by a couple of hours, will cause wilting in the plants and potentially decrease the survivability of the SCN. With manual watering, the person caring for the plants also has to know how much water crocks need based on the plant size and the amount of sun the plants receive. Too much water will inhibit nematode reproduction and too little will result in plant death. Because the amount of water plants receive with the automatic watering system is based on the soil moisture level, watering is automatically adjusted based on sunlight and plant size. Additionally, the automated system can be monitored via the Argus greenhouse control system. If there is a mechanical error and the moisture level drops below a critical level, alarm notices are sent to the greenhouse manager, allowing for human intervention.

Tables and Figures

Figure 2.1. Time graph of the moisture levels of soils in both the automated and manual watering systems. Y-axis is percentage Volumetric Water Content (VWC); X-axis is date.

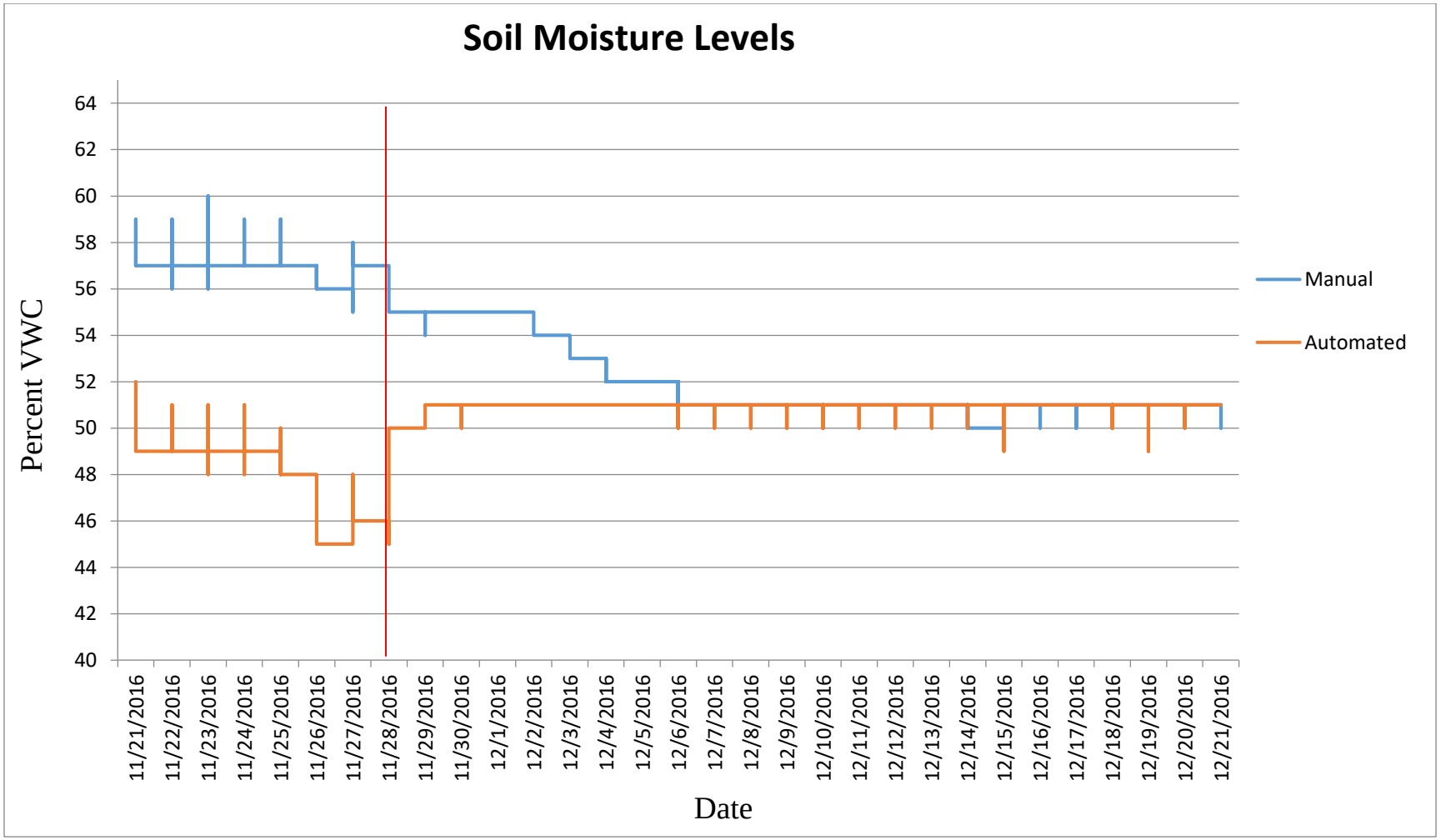

*red line represents when automated watering system was initiated

Table 2.1. Average number of female cysts that formed on the soybean roots of each line for both the automated and manual watering systems.

System	Lee 74*	IA3023*	LD00-2817P	LD00-3309	LD01-5907	Macon*
Manual	132	116	1.1	31	0.5	106
Automated	377	245	1.6	40	0.5	172

***Indicates significant increase of cyst count on line under automated watering system compared to manual hand watering**

Table 2.2. Female indices of the tested lines compared to Lee 74 for both the manual and automated watering systems. Female indices were obtained by taking the number of cysts for the tested lines, divided by the number of cysts on Lee 74 and multiplying by 100. Soybean genotypes with values that are below 10 are considered highly resistance to the SCN population.

		Female Index on Tested Lines				
System	# Females on Lee	IA3023	LD00-2817P	LD00-3309	LD01-5907	Macon
Manual	132	87.7	0.9	23.7	0.4	80.3
Automated	377	65.1	0.4	10.6	0.1	45.7

*Lee 74, IA-3023, and Macon all had a significant increase to cyst counts under the automated watering system compared to manual hand watering

Literature Cited

Arelli, P.R., D.A. Sleper, P. Yue, and J.A. Wilcox. 2000. Soybean reaction to races 1 and 2 of *Heterodera glycines*. Crop Sci. 40: 824-826.

Caviness, C. E., R.D. Riggs, and H.J. Walters. 1974. Registration of Lee 74 soybean. Crop Sci. 15:100.

Concibido, V. C., B.W. Diers, and P.R. Arelli. 2004. A decade of QTL mapping for cyst nematode resistance in soybean. Crop Sci. 44:1121-1131.

Diers, B.W., T. Cary, D. Thomas, A. Colgrove, and T. Niblack. 2010. Registration of LD00-2817P soybean germplasm line with resistance to soybean cyst nematode from PI 437654. J. of Plant Registrations. 4:141-144.

Diers, B.W., T.R. Cary, D.J. Thomas, and C.D. Nickell. 2006. Registration of 'LD00-3309' soybean. Crop Sci. 46:1384.

Heatherly, L.G., L.D. Young, J.M. Epps, and E.E. Hartwig. 1982. Effect of upper-profile soil water potential on numbers of cysts of *Heterodera glycines* on soybeans. Crop Sci. 22:833-835.

Kim, M., D.L. Hyten, A.F. Bent, and B.W. Diers. 2010. Fine mapping of the SCN resistance locus rhg1-b from PI 88788. The Plant Genome J. 3:81-89.

Koenning, S.R., and J.A. Wrather. 2010. Suppression of soybean yield potential in the continental United States by plant diseases from 2006 to 2009. PHP Plant Health Progress. doi:10.1094/php-2010-1122-01-rs

Kopisch-Obuch, F.J., and B.W. Diers. 2005. Segregation at the SCN resistance locus rhg1 in soybean is distorted by an association between the resistance allele and reduced field emergence. Theor Appl Genet. 112:199-207.

Ichinohe, M. 1952. On the soybean nematode, *Heterodera glycines*. Mag. Appl. Zool. 17:1-4

Lauritis, J.A., R.V. Rebois, and L.S. Graney. 1983. Development of *Heterodera glycines Ichinohe* on soybean, *Glycine max L*. Merr., under gnotobiotic conditions. J. Nematology. 15:272-281.

Niblack, T.L., P.R. Arelli, G.R. Noel, C.H. Opperman, J.H. Orf, D.P. Schmitt, J.G. Shannon, and G.L. Tylka. 2002. A revised classification scheme for genetically diverse populations of *Heterodera glycines*. J. Nematology. 34:279-288.

Niblack, T.L. 2005. Soybean cyst nematode management reconsidered. Plant Disease. 89:1020-1026.

Noel, G.R. 1993. *Heterodera gylcines* in soybean. Nematologia Brasileira. 17:103-121.

Riggs, R.D., and D.P. Schmitt. 1988. Complete characterization of the race scheme for *Heterodera glycines*. J. Nematology. 20:392-395.

Wrather, J.A., and S.R. Koenning. 2006. Estimates of disease effects on soybean yields in the United States 2003 to 2005. J. Nematology. 38:173-180.

Young, L.D. 1996. Yield loss in soybean caused by *Heterodera glycines*. J. Nematology. 28:604-607.

Zhang H., C. Li, E.L. Davis, J. Wang, J.D. Griffin, J. Kofsky, B.H. Song. 2016. Genome-wide association study of resistance to soybean cyst nematode (*Heterodera glycines*) HG type 2.5.7 in wild soybean (*Glycine soja*) Front Plant Sci. 7:1214.

CHAPTER 3

Promiscuous Nodulation

Introduction

Soybean [*Glycine max* (L.) Merr.] is an important source of oil and protein for the USA, and has the potential to be a staple crop in Africa because of its high protein concentration and the benefits of the nitrogen fixation from the symbiotic relationship with rhizobium bacteria (Sinclair et al., 2014; Sanginga et al., 2002). For African farmers to benefit from this symbiotic relationship, they need to inoculate soil with *Bradyrhizobium japonicum*, the primary species of bacteria that nodulates soybean, or grow cultivars that nodulate promiscuously. Unfortunately, *B. japonicum* inoculant is often unavailable to small or subsistence farmers in Africa.

While an option, the use of *B. japonicum* inoculants, even when available, may not be best course of action for farmers in Africa. Drought conditions and high temperatures found in tropical environments decrease the survivability of *B. japonicum*, which may make inoculant applications necessary each time a soybean crop is grown (Kueneman, 1984). Responses to *Bradyrhizobium japonicum* inoculant in African soils are often positive, but at times inconsistent depending on factors such as the host plant, the environment, and past field management (Sanginga et al., 1996). These factors have resulted in interest in developing promiscuous soybean cultivars that are compatible with the cowpea strain of rhizobium. The cowpea strain already has a large presence throughout the tropics, and was shown to survive in acidic soils and drought conditions (Kueneman, 1984). Screening for promiscuous nodulation of soybean with indigenous cowpea strains of rhizobium would result in a more sustainable soybean production system. A goal of tropical soybean breeding efforts is to develop highly promiscuous soybean

lines that could match the amount of nitrogen fixation of *B. japonicum*, which can produce 300 kg of N per hectare under ideal circumstances (Keyser and Li, 1992).

Increasing the amount of nitrogen fixed by soybean by breeding promiscuous cultivars that are capable of fixing nitrogen with indigenous rhizobium strains is one of the targeted paths of the International Institute of Tropical Agriculture (IITA) (Kueneman 1984). To meet this goal, it has been important to screen germplasm to identify sources of promiscuous nodulation (Keyser and Li, 1992; Pulver et al., 1985).

Previous germplasm screening work has been done to identify promiscuous soybean lines. Giller et al. (1998) stated that screening for promiscuous nodulation occurred as early as 1981 when 400 soybean lines were tested. Research was then done to develop better methods to screen for promiscuous nodulation, and Gwata et al. (2004) reported that the amount of fixation by promiscuous nodules is correlated with leaf color or greenness. This method will be incorporated in this study to further screen soybean lines for promiscuous nodulation, by using both the "greenness" of the leaves and other factors such nodule number and weight to identify promiscuous lines. The objective of this study was to screen accessions from the soybean germplasm collection for the ability to promiscuously nodulate with the cowpea strain of rhizobium.

Materials and Methods

Accessions were screened for the ability to promiscuously nodulate in greenhouse tests. The majority of the accessions screened were from Asian countries (365 entries), [many being from China (171 entries)], there were some from African countries (49 entries), and Williams 82 from North America was included. Nineteen lines developed at IITA were included in the test because the IITA breeding program develops promiscuously nodulating cultivars.

The plants were grown in vermiculite (BFG Supply [Janesville, WI]) because there are limited nutrients available in this media and therefore would better show nitrogen deficiency symptoms when nodulation is ineffective. To prevent contamination of *Bradyrhizobium japonicum* in the tests, all seed, soil, and pots were sterilized. The vermiculite was sterilized in Bel-Art SP Scienceware Clavies High-Temperature Autoclave Bags (Fisher Science [Pittsburg, PA]) that were autoclaved at 20 PSI and 127°C for 2 hours before planting. The accessions were planted in 15 cm diameter plastic pots, one accession per pot, that were sterilized before planting by dipping in a ZeroTol 2.0 (BioSafe Systems L.L.C, East Hartford, CT) solution mixed at a ratio of 1:100 ZeroTol to water. The ZeroTol was additionally sprayed on the work area used for planting.

Before planting the seeds, 6 g of granular peat inoculant was spread evenly in a 2.5 cm hole dug into the vermiculite media in each pot. This inoculant was the USDA3456 strain of cowpea inoculant provided by Patrick Elia, USDA-ARS. The seeds were placed on top of the inoculant to allow the roots to grow directly through the inoculant. Fifteen seeds from each accession were planted, unless a limitation on available seed prevented this. Prior to planting, seeds were sterilized for 10 minutes in a 5% sodium hypochlorite solution, using Clorox bleach as the source of hypochlorite (The Clorox Company, Oakland, CA). Seeds were then immediately triple washed in distilled water and sown into the vermiculite.

In a greenhouse, the pots were placed into 27x42x6 cm water basins that were sterilized with the ZeroTol 2.0 solution described above. Greenhouse condition were set to approximately 28°C/20°C day/night temperatures, and a 14-hour day length. The water basins were used to both water and fertilize the plants. The plants were fertilized days 14, 21, and 28 after planting by adding 150 mL of a 5 X modified Hoagland solution minus nitrogen (Imsande, 1981) per pot to

the water basins, which each typically had six pots. Thirty four days after planting, the plants in each pot were visually scored for their chlorosis level (Gwata et al. 2004) using a score of 1-5, with 1 given to pots that lacked nearly all chlorophyll and 5 for pots showing no signs of chlorosis (Figure 3.1). The number of plants that germinated in each pot was also recorded.

After the plants were scored for chlorosis, they were uprooted, and the nodules were removed, checked for effectiveness, counted, dried, and weighed (these figures were done on a whole pot basis). The nodules were first tested for the presence of leghemoglobin by breaking open a nodule from each accession and scoring it for the presence of red/pinkish coloration. Nodules with the red/pinkish coloration were scored as effective. Nodules were then hand counted by removing them from the roots, and stored in paper coin envelopes (this measurement is not size dependent). All the paper coin envelopes containing the nodules were then placed in a dryer for four days at 30°C. After this drying period, they were weighted using a Mettler PM4000 balance [Mettler-Toledo (Greifensee, Switzerland)].

Results

Because the goal of this experiment was to screen a large amount of germplasm to identify accessions that are potential sources of the promiscuous nodulation trait, only one replication of testing was performed for each accession. Correlations between nodulation traits were examined (Table 3.1). Because inconsistent emergence resulted in the number of plants varying from pot to pot, it was important to consider the correlation between the number of plants in pots and other traits. The chlorosis index (CI) was positively correlated with all of the nodulation traits, which was expected as this shows that on average, the more green plants were, the more nodulation and effective nodulation occurred. Nodule count and weight was determined both on a pot and plant basis and these values on a pot basis were more highly correlated with CI

than the values on a plant basis. The highest correlation with CI for the traits measured was nodule weight, followed by nodule count and effective nodules.

The results were further examined by dividing lines into four groups based on the average number of nodules formed on a plant basis for each line (Table 3.2). The none group had no nodule formation, and low, medium, high, were roughly broken up into three groups with similar numbers of accessions. These groups were broken up evenly because of the lack of reference genotypes for defining groups. The high group provided further evidence that the CI was correlated with the average number of nodules (Table 3.2). Nearly half of the lines in the high group were a ranked a 5 on the CI scale, meaning they were fully green and showed no signs of chlorosis. As other groups were considered, the number of accessions that received CI rating of 5 and 4 dropped rapidly. Inversely, the majority of high average nodule counts tended to be in the higher CI ranks (Figure 3.1). There was also strong correlation between the nodule weights and nodule counts, and the average nodule weights and nodule counts (Table 3.1).

There were 42 accessions with CI values of 5, meaning they showed no chlorosis. Of these accessions, 19 were from China, eight from India, four from Indonesia, three from Japan, two from Nigeria, six from Vietnam and one from Zimbabwe. The accession that produced the greatest number of nodules was PI 429330, which was collected in Nigeria. This accession had 174 nodules and an average of 21.75 nodules plant^{-1} (Table 3.3). These nodules were rated as effective, and the accession had a CI of 5. The name of this accession is TGM 618, and it was developed by IITA, which suggests that it was likely developed to nodulate promiscuously. Other lines that were able to produce a high number of average nodules were PI587860, PI606419, and PI603563C.

Nodule weight was highly correlated with nodule counts (Table 3.1), due primarily to an increase in nodule number resulting in an increase in the overall weight of nodules per line. Because of this, evaluation based on the average weights of the nodules would be more effective than using the total nodule weights. Accession PI281883C had an average nodule weight of 90.6 milligrams^{-1} (Table 3.3), while not the heaviest nodules in the study, it had the heaviest nodules for any accession with a CI score of 5. PI281883C, which was collected from Indonesia, also had an average of 16 nodules plant^{1}.

Fourteen accessions were selected for inclusion in this study based on references in the literature that indicated that they may promiscuously nodulate (Keyser and Li, 1992; Pulver et al., 1985), (these lines are highlighted on Table 3.3). Of these accessions, one had a CI of 5 and two had CI values for 4. One of these accessions with a CI value of 4 was not nodulated. The IITA lines emerged poorly, and no plants emerged for eight of the lines. The low These IITA lines did not nodulate well in the test with only one line having a CI of 4, six with CI of 3 and four with CI of 2. Further research is needed to determine why these accessions and lines that were predicted to nodulate well were poorly nodulated. It is possible that they could respond better to other strains of cowpea rhizobium.

Discussion

This test was a preliminary screening of germplasm to identify new sources of promiscuous nodulation. From this preliminary single replication test, accessions that showed little to no leaf chlorosis and good nodulation were identified. These accessions will need to be retested in replicated experiments to verify these results and to eliminate the possibility that nodulation was not the result of contamination with *B. japonicum*. Accessions with verified

promiscuous nodulation could then be tested to determine if they have unique genes controlling this trait.

Of the 19 IITA lines that early showed evidence of promiscuous nodulation in previous screenings, only 5 successfully nodulated in this study. The theory behind this low number being able to nodulate in this study was the due to the strain of cowpea rhizobia used. The lines may have not been able to nodulate with this specific stain used.

Some correlations were apparent between nodulations traits, such as the nodule weights and nodule counts, and the average nodule weights and nodule counts. The total nodule weight and the nodule counts showed a strong correlation, as expected, but the average nodule weight and nodule counts did as well. The average nodule weights seemed to decrease in average weight as the number of nodules present increased. Further research would be needed to evaluate this trend.

Correlations with CI are important in this study as it is our method to visually evaluate nitrogen fixation. CI was significantly correlated with average nodule count, average nodule weight, and effective nodulation (Table 3.1), which are all important traits for lines to efficiently fix nitrogen. CI is a useful trait, but not a perfect method for evaluating nitrogen fixation, as a few lines were able to score 4 and 5 while having no to very few effective nodules (Table 3.3), though these lines were shown to be outliers (Figure 3.2). Theories on how these lines maintained the high CI level while under nitrogen stress are that they are genetically better at coping with nitrogen stress, and some of the pots with these lines had fewer plants to emerge, further enabling the lines to reduce nitrogen stress. Overall, despite these outliers, CI still is an effective preliminary screening method to identify germplasm that can fix nitrogen by nodulation with the cowpea strain of rhizobium bacteria.

Tables and Figures

Figure 3.1. A representation of the scale used for the chlorosis index. From left to right, rank 5-1.

Figure 3.2. Box plots of the chlorosis index and average number of nodules per plant.

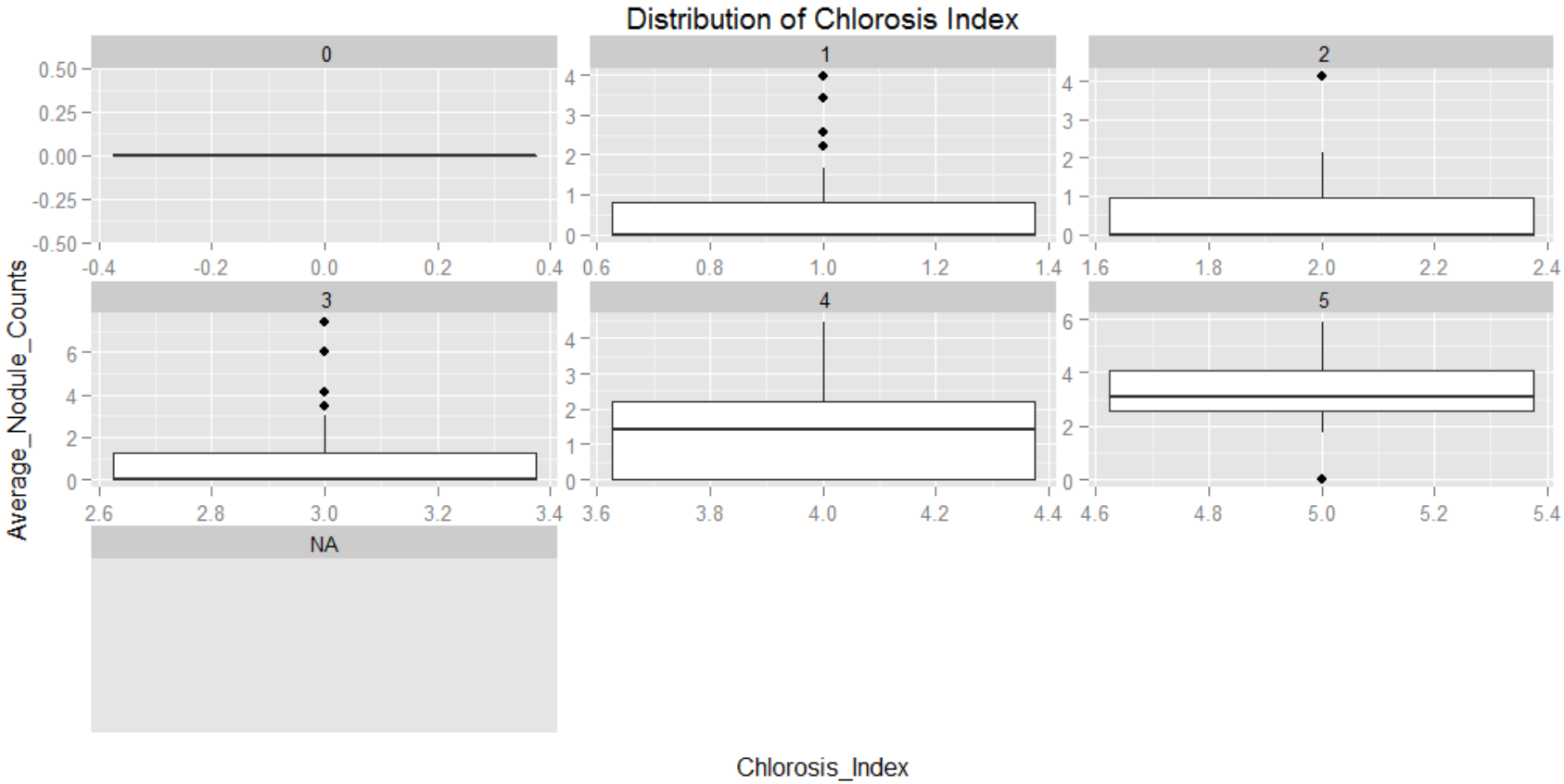

Table 3.1. Correlation values for promiscuous nodulation traits. Chlorosis index is a 1-5 scale with 1 = fully bleached and 5 = no signs of chlorosis, effective nodules is a rating of whether the nodules have red/pinkish cores which is associated with the ability to fix nitrogen, nodule counts are the number of nodules that formed in a pot, nodule weight is the dry weight of all the nodules found in the pot, and average count is the number of nodules on a single soybean plant basis and average nodule weight is the average dry weight of individual nodules.

	Plant Count	Chlorosis Index	Effective Nodules	Nodule Counts	Average Count	Nodule Weight	Average Nodule Weight
Plant Count	-	0.18	0.12	0.16	-0.10	0.14	-0.10
Chlorosis Index		-	0.44	0.47	0.38	0.53	0.38
Effective Nodules‡			-	0.52	0.44	0.58	0.44
Nodule Counts				-	0.74	0.85	0.74
Average Count					-	0.62	1.00
Nodule Weight						-	0.62
Average Nodule Weight							-

†All correlation values are significant
‡Effective nodules were run as a binary presence absent format, with presence of red/pinkish coloration as 1 and no red/pinkish coloration as 0

Table 3.2. Distribution of chlorosis index (CI) values after separating soybean accessions into four groups based on average nodule count per plant.

Distribution of the Chlorosis Index

Average Count Level	Mean	Median	Mode	Percentage with a CI of 5	Percentage with a CI of 4+
High	4.083	4	5	47%	74%
Medium	3.286	3	3	6%	41%
Low	2.653	3	3	0%	15%
None	2.201	2	3	2%	12%
Average†	2.768	3	3	10%	28%

† Average for all data not separated into groups.

Table 3.3. Ratings of accessions from the nodulation test. Plant count is the number of plants in the pot and evaluated for the line. Chlorosis index measures the chlorosis level of each accession with 1 = fully bleached and 5 = no signs of chlorosis. Effective nodules is a rating for the presence of leghemoglobin, 1 = red/pinkish color in the core of the tested nodule indicating the presence of leghemoglobin and 0 = brown core indicating no leghemoglobin present. Nodule number is the number of nodules on a whole pot basis. Nodule weights (milligrams) are the dry weight of nodules on a whole pot basis. Average count plant^{-1} is the average number of number of nodules on a plant basis and average weight nodule^{-1} is the average dry weight of individual nodules. Highlighted rows are fourteen accessions selected for previous indication for promiscuous nodulation.

acid	Province	Country	MG	Plant Count	Chlorosis Index (1-5)	Effective Nodules	Nodule Number	Nodule Weights (mg)	Average Nodule Number Plant^{-1}	Average Weight nodule^{-1} (mg)
PI429330	unknown	Nigeria	VIII	8	5	1	174	470	21.75	2.70
PI567365	Ningxia	China	III	11	5	1	145	400	13.18	2.76
PI475822B	Xinjiang	China	III	8	5	1	134	500	16.75	3.73
PI606367	(north)	Vietnam	VIII	8	5	1	133	340	16.63	2.56
PI475818	Xinjiang	China	III	8	5	1	110	230	13.75	2.09
PI578449	Minh Hai	Vietnam	IX	7	5	1	104	580	14.86	5.58
PI374189	Madhya Pradesh	India	X	9	5	1	102	320	11.33	3.14
PI429329	unknown	Nigeria	VII	5	5	1	94	290	18.80	3.09
PI307882A	Madhya Pradesh	India	IX	5	5	1	93	520	18.60	5.59
PI606419	(north)	Vietnam	VIII	4	5	1	92	300	23.00	3.26
PI497957	Bihar	India	X	11	5	1	91	350	8.27	3.85
PI086006	Hokkaido	Japan	III	9	5	1	82	220	9.11	2.68
PI605823	Ha giang	Vietnam	IX	8	5	1	76	300	9.50	3.95
PI549019	Ningxia	China	V	11	5	1	75	160	6.82	2.13
PI307896	Madhya Pradesh	India	IX	6	5	1	74	520	12.33	7.03
PI603596	Fujian	China	III	8	5	1	73	450	9.13	6.16
PI497952	Bihar	India	X	7	5	1	71	260	10.14	3.66
PI603563C	Shanxi	China	V	3	5	1	70	160	23.33	2.29
PI567388	Shaanxi	China	V	10	5	1	69	250	6.90	3.62
PI567343	Gansu	China	V	7	5	1	68	270	9.71	3.97

Table 3.3. (cont.)

acid	Province	Country	MG	Plant Count	Chlorosis Index	Effective Nodules	Nodule Number	Nodule Weights	Average Number Plant^{-1}	Average Weight nodule^{-1}
PI567303B	Gansu	China	V	7	5	1	66	110	9.43	1.67
PI281883C	unknown	Indonesia	X	4	5	1	64	580	16.00	9.06
PI175174	Uttar Pradesh	India	VI	7	5	1	58	120	8.29	2.07
PI567568B	Shandong	China	V	5	5	1	57	180	11.40	3.16
PI171438	Sichuan	China	VII	11	5	1	55	270	5.00	4.91
PI606412	(north)	Vietnam	V	3	5	1	54	190	18.00	3.52
PI307882E	Madhya Pradesh	India	IX	9	5	1	48	220	5.33	4.58
PI441381	Java	Indonesia	VIII	6	5	1	48	260	8.00	5.42
PI567074A	East Java	Indonesia	VIII	10	5	1	41	240	4.10	5.85
PI232992	Saga	Japan	III	2	5	1	37	160	18.50	4.32
PI587860	Zhejiang	China	V	1	5	1	35	120	35.00	3.43
PI175188	Uttar Pradesh	India	VII	2	5	1	34	30	17.00	0.88
PI499955	Sichuan	China	VII	5	5	1	32	250	6.40	7.81
PI567342	Gansu	China	V	3	5	1	27	110	9.00	4.07
PI594890	Yunnan	China	VII	2	5	1	24	140	12.00	5.83
PI441359	Java	Indonesia	VIII	6	5	1	24	200	4.00	8.33
PI476892	(north)	Vietnam	VIII	5	5	1	19	120	3.80	6.32
PI548469	unknown	Japan	VII	5	5	1	15	180	3.00	12.00
PI476898	unknown	China	VIII	1	5	0	0	0	0.00	0.00
PI587583D	Jiangsu	China	VII	2	5	0	0	0	0.00	0.00
PI594457A	Sichuan	China	III	10	5	0	0	0	9.43	1.67
PI603530C	Shaanxi	China	V	3	5	0	0	0	16.00	9.06
PI594885A	Yunnan	China	V	7	4.5	1	24	140	8.29	2.07
PI417054	Tohoku	Japan	III	4	4.5	1	12	100	11.40	3.16
PI594770B	Guangxi	China	VIII	5	4	1	100	330	5.00	4.91
PI391586	Liaoning	China	III	11	4	1	84	150	18.00	3.52

Table 3.3. (cont.)

acid	Province	Country	MG	Plant Count	Chlorosis Index	Effective Nodules	Nodule Number	Nodule Weights	Average Number Plant^{-1}	Average Weight nodule^{-1}
PI615450	Ca Mau	Vietnam	X	7	4	1	82	520	11.71	6.34
PI578460	(north)	Vietnam	VIII	5	4	1	79	340	15.80	4.30
PI567257C	Jiangxi	China	VIII	9	4	1	66	360	7.33	5.45
PI567315	Gansu	China	VII	5	4	1	59	280	11.80	4.75
PI326578	unknown	China	VIII	5	4	1	51	160	10.20	3.14
PI407769	Guangdong	China	VIII	3	4	1	51	300	17.00	5.88
PI605862B	Hai hung	Vietnam	VI	4	4	1	48	200	12.00	4.17
PI381682	unknown	Uganda	VII	6	4	1	46	130	7.67	2.83
PI203399	unknown	Japan	VIII	9	4	1	43	300	4.78	6.98
PI567595A	Shandong	China	III	9	4	1	42	190	4.67	4.52
PI567107A	East Java	Indonesia	VIII	7	4	1	42	250	6.00	5.95
PI429328	unknown	Nigeria	VIII	11	4	1	41	190	3.73	4.63
PI594839A	Yunnan	China	VIII	8	4	1	39	180	4.88	4.62
PI567250B	Hunan	China	III	11	4	1	39	200	3.55	5.13
PI240671	Luzon	Philippines	VIII	6	4	1	31	330	5.17	10.65
PI468967	unknown	Vietnam	V	6	4	1	30	170	5.00	5.67
PI603588	Shanxi	China	V	8	4	1	29	130	3.63	4.48
PI567071A	East Java	Indonesia	IX	12	4	1	28	200	2.33	7.14
PI567377A	Shaanxi	China	V	5	4	1	27	110	5.40	4.07
PI594792A	Yunnan	China	V	6	4	1	23	260	3.83	11.30
PI587992C	Sichuan	China	VII	7	4	1	19	100	11.71	6.34
PI567130C	East Java	Indonesia	IX	3	4	1	19	60	15.80	4.30
PI594662B	Guizhou	China	V	5	4	1	18	90	7.33	5.45
PI200478	Shikoku	Japan	III	9	4	1	17	200	11.80	4.75
PI561382	Jiangxi	China	VII	6	4	1	16	130	10.20	3.14
PI407746	Shanghai	China	III	6	4	1	12	110	17.00	5.88

Table 3.3. (cont.)

acid	Province	Country	MG	Plant Count	Chlorosis Index	Effective Nodules	Nodule Number	Nodule Weights	Average Number Plant^{-1}	Average Weight nodule^{-1}
PI567015	unknown	Indonesia	IX	2	4	1	12	120	6.00	10.00
PI221715	North West	South Africa	VII	5	4	1	10	60	2.00	6.00
PI437734	unknown	China	V	6	4	1	9	70	1.50	7.78
PI441353	Java	Indonesia	VIII	3	4	1	9	30	3.00	3.33
TGX 1937-1F				3	4	1	9	70	3.00	7.78
PI518295	unknown	Taiwan	VII	2	4	1	8	80	4.00	10.00
PI548444	Zhejiang	China	VIII	6	4	1	7	100	1.17	14.29
PI407761	Shanghai	China	V	3	4	1	7	60	2.33	8.57
PI171450	Kagoshima	Japan	III	5	4	1	7	10	1.40	1.43
PI587567A	Jiangsu	China	VII	6	4	1	6	40	1.00	6.67
PI587633A	Jiangsu	China	VII	3	4	1	6	90	2.00	15.00
PI341251	unknown	Taiwan	IX	4	4	1	6	40	1.50	6.67
PI594846	Yunnan	China	VIII	2	4	1	4	10	2.00	2.50
PI567017A	unknown	Indonesia	VIII	1	4	1	4	10	4.00	2.50
PI416892	Hokuriku	Japan	III	5	4	1	3	>10	0.60	>10
PI548447	Zhejiang	China	VIII	8	4	1	2	>10	0.25	>10
PI594904	Sichuan	China	VII	5	4	1	2	50	0.40	25.00
PI200498	unknown	China	VII	5	4	1	1	>10	0.20	>10
PI603674	Jiangsu	China	III	4	4	1	1	10	0.25	10.00
PI594568A	Jiangxi	China	V	6	4	1	1	>10	0.17	>10
PI507491	Tohoku	Japan	III	5	4	0	0	0	6.00	10.00
PI548489	Zhejiang	China	VIII	2	4	0	0	0	2.00	6.00
PI587568A	Jiangsu	China	VII	2	4	0	0	0	1.50	7.78
PI594751B	Guangxi	China	VII	2	4	0	0	0	3.00	3.33
PI090392	Tianjin	China	III	1	4	0	0	0	3.00	7.78
PI561271	Zhejiang	China	V	3	4	0	0	0	4.00	10.00

Table 3.3. (cont.)

acid	Province	Country	MG	Plant Count	Chlorosis Index	Effective Nodules	Nodule Number	Nodule Weights	Average Number Plant^{-1}	Average Weight nodule^{-1}
PI567521	Shandong	China	V	1	4	0	0	0	0.00	0.00
PI567759	Jiangsu	China	V	7	4	0	0	0	0.00	0.00
PI594567D	Jiangxi	China	V	12	4	0	0	0	0.00	0.00
PI603578	Shanxi	China	V	5	4	0	0	0	0.00	0.00
PI603677A	Jiangsu	China	V	6	4	0	0	0	0.00	0.00
PI323555	Uttar Pradesh	India	IV	11	4	0	0	0	0.00	0.00
PI567009A	unknown	Indonesia	VIII	1	4	0	0	0	0.00	0.00
PI417047	Hokuriku	Japan	VII	2	4	0	0	0	0.00	0.00
PI506975	Kanto	Japan	VII	3	4	0	0	0	0.00	0.00
PI084973	Saitama	Japan	III	8	4	0	0	0	0.00	0.00
PI379559D	Hyogo	Japan	III	5	4	0	0	0	0.00	0.00
PI506529	Tohoku	Japan	III	3	4	0	0	0	0.00	0.00
PI504492	unknown	Taiwan	00	11	4	0	0	0	0.00	0.00
PI606431	(north)	Vietnam	VIII	6	4	0	0	0	0.00	0.00
PI145079	unknown	Zimbabwe	VII	1	4	0	0	0	0.00	0.00
PI566957	East Java	Indonesia	IX	6	3.5	1	15	140	2.50	9.33
PI567071B	East Java	Indonesia	IX	10	3.5	1	21	60	2.10	2.86
PI346306	unknown	India	V	9	3	1	150	220	16.67	1.47
PI578451	(north)	Vietnam	IV	2	3	1	111	150	55.50	1.35
PI303652	unknown	China	V	11	3	1	97	200	8.82	2.06
PI548468	Mississippi	United States	VIII	5	3	1	60	240	0.00	0.00
PI307880A	Madhya Pradesh	India	IX	1	3	1	55	80	0.00	0.00
PI603560	Shanxi	China	III	9	3	1	42	110	0.00	0.00
PI229336	Kyushu	Japan	III	8	3	1	40	100	0.00	0.00
PI578439	(north)	Vietnam	III	6	3	1	40	160	0.00	0.00
PI171449	Niigata	Japan	III	6	3	1	39	110	0.00	0.00

Table 3.3. (cont.)

acid	Province	Country	MG	Plant Count	Chlorosis Index	Effective Nodules	Nodule Number	Nodule Weights	Average Number Plant^{-1}	Average Weight nodule^{-1}
PI587597C	Jiangsu	China	VIII	5	3	1	35	130	7.00	3.71
PI086081	Hokkaido	Japan	III	6	3	1	31	150	5.17	4.84
PI605861A	Hai hung	Vietnam	VII	4	3	1	31	160	7.75	5.16
PI393546	unknown	Taiwan	VIII	9	3	1	30	60	3.33	2.00
PI603442	Nei Monggol	China	III	12	3	1	29	100	2.42	3.45
PI374192A	Madhya Pradesh	India	IX	7	3	1	27	180	3.86	6.67
PI175191	Uttar Pradesh	India	VII	8	3	1	24	50	3.00	2.08
PI170896	North West	South Africa	V	6	3	1	24	70	4.00	2.92
PI587601E	Jiangsu	China	VII	8	3	1	23	60	2.88	2.61
PI221714	North West	South Africa	VI	11	3	1	23	100	2.09	4.35
PI200548	Shikoku	Japan	III	7	3	1	20	>10	2.86	>10
PI163308	Himachal Pradesh	India	X	4	3	1	19	60	4.75	3.16
PI438282B	unknown	Japan	VII	7	3	1	19	30	2.71	1.58
PI507487	Tohoku	Japan	III	3	3	1	19	200	6.33	10.53
PI605761	Lang son	Vietnam	VIII	6	3	1	18	50	3.00	2.78
PI605833	Ha giang	Vietnam	IX	9	3	1	17	90	1.89	5.29
PI504490	unknown	Taiwan	II	4	3	1	16	80	4.00	5.00
PI603438E	Nei Monggol	China	III	9	3	1	14	60	1.56	4.29
PI567097B	East Java	Indonesia	VIII	4	3	1	14	70	3.50	5.00
PI507024	Kyushu	Japan	VII	8	3	1	14	70	1.75	5.00
PI518757	unknown	Taiwan	III	5	3	1	14	140	7.00	3.71
PI587622B	Jiangsu	China	VII	6	3	1	12	80	5.17	4.84
PI567347	Gansu	China	V	9	3	0	11	10	7.75	5.16
PI464877	Jilin	China	III	11	3	1	10	50	3.33	2.00
PI566992B	unknown	Indonesia	VI	3	3	1	10	40	2.42	3.45
PI587695	Anhui	China	VII	9	3	1	9	120	3.86	6.67

Table 3.3. (cont.)

acid	Province	Country	MG	Plant Count	Chlorosis Index	Effective Nodules	Nodule Number	Nodule Weights	Average Number Plant^{-1}	Average Weight nodule^{-1}
PI245008		Uganda	VIII	1	3	1	9	10	9.00	1.11
PI605827B	Ha giang	Vietnam	V	12	3	1	9	20	0.75	2.22
PI445845	Zhejiang	China	III	9	3	1	7	160	0.78	22.86
TGX 1440-1E				2	3	1	7	20	3.50	2.86
PI088292	Jilin	China	III	10	3	1	6	20	0.60	3.33
PI567054B	unknown	Indonesia	VIII	4	3	1	6	50	1.50	8.33
PI417198	Tohoku	Japan	III	5	3	1	6	10	1.20	1.67
PI434973A	unknown	Nigeria	IX	9	3	1	6	60	0.67	10.00
WILLIAMS 82	Illinois	United States	III	6	3	0	6	>10	1.00	>10
PI549018	Ningxia	China	V	5	3	1	5	>10	1.00	>10
PI240667A	Luzon	Philippines	IX	5	3	1	5	20	1.00	4.00
PI240667B	Luzon	Philippines	IX	8	3	1	5	40	0.63	8.00
PI538377	Hebei	China	III	9	3	1	4	30	0.44	7.50
PI507017	Kanto	Japan	VII	9	3	1	4	20	0.44	5.00
TGX 1989-19F				4	3	1	4	40	1.00	10.00
PI079861	Heilongjiang	China	VII	6	3	1	3	10	0.50	3.33
PI091341	Hebei	China	III	7	3	1	3	20	0.43	6.67
PI578491B	Henan	China	V	2	3	1	3	10	1.50	3.33
PI307843A	Madhya Pradesh	India	IX	9	3	1	3	80	0.33	26.67
PI567121B	East Java	Indonesia	IX	1	3	1	3	10	3.00	3.33
PI506592	Tohoku	Japan	III	4	3	1	3	10	9.00	1.11
PI381662	unknown	Uganda	VI	7	3	1	3	10	0.75	2.22
PI548472	Jiangsu	China	VII	5	3	1	2	10	0.78	22.86
PI587815A	Hubei	China	VII	2	3	1	2	10	3.50	2.86
PI468914	Liaoning	China	III	4	3	1	2	>10	0.60	3.33
PI470227B	Liaoning	China	III	10	3	1	2	10	1.50	8.33

Table 3.3. (cont.)

acid	Province	Country	MG	Plant Count	Chlorosis Index	Effective Nodules	Nodule Number	Nodule Weights	Average Number Plant^{-1}	Average Weight nodule^{-1}
FC031592	unknown	Indonesia	VIII	5	3	1	2	>10	0.40	>10
PI203404	unknown	Japan	VII	3	3	1	2	10	0.67	5.00
PI376070	unknown	Cameroon	VII	9	3	0	1	>10	0.11	>10
PI548464	Tianjin	China	V	7	3	1	1	>10	0.14	>10
PI346298	unknown	India	VII	3	3	1	1	>10	0.33	>10
PI605792D	Cao bang	Vietnam	IV	1	3	1	1	>10	1.00	>10
TGX 1987-62F				2	3	1	1	>10	0.50	>10
PI341245	unknown	Tanzania	IX	10	3	0	0	0	0.00	0.00
PI476933	(north)	Vietnam	V	6	3	0	0	0	0.00	0.00
PI509113	Yunnan	China	VII	3	3	0	0	0	0.00	0.00
PI532458	Shanxi	China	VIII	10	3	0	0	0	0.00	0.00
PI587632B	Jiangsu	China	VII	2	3	0	0	0	0.00	0.00
PI587889	Zhejiang	China	VIII	7	3	0	0	0	0.00	0.00
PI594793	Yunnan	China	VII	6	3	0	0	0	0.00	0.00
PI594879	Yunnan	China	VIII	1	3	0	0	0	0.00	0.00
PI603641	Hubei	China	VIII	5	3	0	0	0	0.00	0.00
PI088289	Jilin	China	III	8	3	0	0	0	0.00	0.00
PI088305	Liaoning	China	III	6	3	0	0	0	0.00	0.00
PI088788	Liaoning	China	III	6	3	0	0	0	0.00	0.00
PI464914B	Liaoning	China	III	8	3	0	0	0	0.00	0.00
PI468384	Jilin	China	III	3	3	0	0	0	0.40	>10
PI532462A	Hebei	China	III	5	3	0	0	0	0.67	5.00
PI548316	Zhejiang	China	III	6	3	0	0	0	0.11	>10
PI549021A	Liaoning	China	III	12	3	0	0	0	0.14	>10
PI549031	Beijing	China	III	11	3	0	0	0	0.33	>10
PI567583A	Shandong	China	III	11	3	0	0	0	1.00	>10

Table 3.3. (cont.)

acid	Province	Country	MG	Plant Count	Chlorosis Index	Effective Nodules	Nodule Number	Nodule Weights	Average Number Plant^{-1}	Average Weight nodule^{-1}
PI567729	Anhui	China	III	11	3	0	0	0	0	0
PI567774B	Jiangsu	China	III	10	3	0	0	0	0	0
PI574480B	Liaoning	China	III	11	3	0	0	0	0	0
PI594394	Anhui	China	III	11	3	0	0	0	0	0
PI548439	Hebei	China	V	9	3	0	0	0	0	0
PI587848	Hubei	China	V	4	3	0	0	0	0	0
PI594614B	Guizhou	China	V	7	3	0	0	0	0	0
PI594656	Guizhou	China	V	4	3	0	0	0	0	0
PI594784B	Yunnan	China	V	9	3	0	0	0	0	0
PI594856	Yunnan	China	V	9	3	0	0	0	0	0
PI594864	Yunnan	China	V	5	3	0	0	0	0	0
PI603693A	Jiangsu	China	V	7	3	0	0	0	0	0
PI307891A	Madhya Pradesh	India	IX	10	3	0	0	0	0	0
PI428691	Manipur	India	VIII	4	3	0	0	0	0	0
PI578486	Uttarakhand	India	III	8	3	0	0	0	0	0
PI567045	South Sulawesi	Indonesia	IX	4	3	0	0	0	0	0
PI567048A	unknown	Indonesia	VIII	1	3	0	0	0	0	0
PI200464	Shikoku	Japan	VII	3	3	0	0	0	0	0
PI200528	Shikoku	Japan	VIII	9	3	0	0	0	0	0
PI200542	Shikoku	Japan	VII	4	3	0	0	0	0	0
PI230971	unknown	Japan	VIII	8	3	0	0	0	0	0
PI230972	unknown	Japan	VIII	3	3	0	0	0	0	0
PI284873	Chiba	Japan	VIII	8	3	0	0	0	0	0
PI378693A	Miyagi	Japan	VIII	8	3	0	0	0	0	0
PI417428	Kanto and Tosan	Japan	VIII	11	3	0	0	0	0	0
PI506548	Kanto	Japan	VII	8	3	0	0	0	0	0

Table 3.3. (cont.)

acid	Province	Country	MG	Plant Count	Chlorosis Index	Effective Nodules	Nodule Number	Nodule Weights	Average Number Plant^{-1}	Average Weight nodule^{-1}
PI507058	Kanto	Japan	VII	2	3	0	0	0	0	0
PI567176	unknown	Japan	VII	2	3	0	0	0	0	0
PI080459	unknown	Japan	III	1	3	0	0	0	0	0
PI196149	unknown	Japan	III	5	3	0	0	0	0	0
PI417297	Kanto and Tosan	Japan	III	10	3	0	0	0	0	0
PI506527	Tohoku	Japan	III	9	3	0	0	0	0	0
PI507171	Kanto	Japan	III	9	3	0	0	0	0	0
PI210352	unknown	Mozambique	VII	10	3	0	0	0	0	0
PI310439	unknown	Papua New Guinea	VII	3	3	0	0	0	0	0
PI324924	unknown	South Africa	V	7	3	0	0	0	0	0
PI159319	North West	South Africa	V	7	3	0	0	0	0	0
PI330635	unknown	South Africa	VII	1	3	0	0	0	0	0
PI504483A	unknown	Taiwan	00	8	3	0	0	0	0	0
PI504489	unknown	Taiwan	I	9	3	0	0	0	0	0
PI341242	unknown	Tanzania	IX	9	3	0	0	0	0	0
PI341247	Tabora	Tanzania	IX	9	3	0	0	0	0	0
WILLIAMS 82	Illinois	United States	III	6	3	0	0	0	0	0
WILLIAMS 82	Illinois	United States	III	3	3	0	0	0	0	0
PI476926	(north)	Vietnam	VII	6	3	0	0	0	0	0
PI567183	unknown	Vietnam	V	6	3	0	0	0	0	0
PI605767B	Lang son	Vietnam	VIII	1	3	0	0	0	0	0
PI605828B	Ha giang	Vietnam	IV	5	3	0	0	0	0	0
PI606364	(north)	Vietnam	V	7	3	0	0	0	0	0
TGX 1448-2E				6	3	0	0	0	0	0
TGX 1805-31F				7	3	0	0	0	0	0
TGX 1987-14F				2	3	0	0	0	0	0

Table 3.3. (cont.)

acid	Province	Country	MG	Plant Count	Chlorosis Index	Effective Nodules	Nodule Number	Nodule Weights	Average Number Plant^{-1}	Average Weight nodule^{-1}
PI368037	unknown	Taiwan	VI	9	2.5	1	6	10	0.67	1.67
PI587563A	Jiangsu	China	VII	2	2	1	34	80	17.00	2.35
PI605758A	Lang son	Vietnam	VIII	8	2	1	33	130	4.13	3.94
PI504497	unknown	Taiwan	II	8	2	1	24	140	3.00	5.83
PI072232	Jiangxi	China	III	5	2	1	23	80	4.60	3.48
PI307868	Madhya Pradesh	India	X	5	2	1	22	100	4.40	4.55
PI594307	Chiba	Japan	VIII	12	2	1	21	20	1.75	0.95
PI434980A	unknown	Central African Republic	VIII	7	2	1	19	130	2.71	6.84
PI561381	Jiangxi	China	VII	10	2	1	15	180	1.50	12.00
PI205086	unknown	Japan	III	8	2	1	15	150	1.88	10.00
PI587719B	Hubei	China	V	5	2	1	14	60	2.80	4.29
PI588011A	Sichuan	China	V	5	2	1	14	50	2.80	3.57
PI549026	Liaoning	China	V	5	2	0	13	50	2.60	3.85
PI346309	unknown	India	V	5	2	1	12	70	2.40	5.83
PI379561	Hyogo	Japan	III	7	2	0	12	>10	1.71	>10
PI603428D	Nei Monggol	China	III	11	2	1	10	30	0.91	3.00
PI393545	unknown	Taiwan	VIII	7	2	1	10	10	1.43	1.00
TGX 1991-10F				7	2	1	9	40	1.29	4.44
PI603631	Hubei	China	VII	8	2	1	8	50	1.00	6.25
PI476929	(north)	Vietnam	VI	9	2	0	8	10	0.89	1.25
PI594805A	Yunnan	China	VII	6	2	1	6	20	0.67	1.67
PI479729	Jilin	China	III	10	2	1	6	10	17.00	2.35
PI506607	Kyushu	Japan	VIII	6	2	1	5	20	4.13	3.94
TGX 1904-6F				4	2	1	4	20	3.00	5.83
PI587882	Zhejiang	China	VII	10	2	1	2	50	4.60	3.48
PI241424	Hokkaido	Japan	VII	7	2	1	2	>10	4.40	4.55

Table 3.3. (cont.)

acid	Province	Country	MG	Plant Count	Chlorosis Index	Effective Nodules	Nodule Number	Nodule Weights	Average Number Plant^{-1}	Average Weight nodule^{-1}
PI567069A	East Java	Indonesia	VIII	8	2	1	1	>10	0.13	>10
PI504499	unknown	Taiwan	000	3	2	1	1	>10	0.33	>10
PI381663	unknown	Uganda	VI	6	2	0	1	0	0.17	0.00
TGX 1990-67F				6	2	1	1	10	0.17	10.00
PI587615	Jiangsu	China	VII	7	2	0	0	0	0.00	0.00
PI587681	Anhui	China	VII	8	2	0	0	0	0.00	0.00
PI588014C	Sichuan	China	VII	7	2	0	0	0	0.00	0.00
PI588017C	Sichuan	China	VII	6	2	0	0	0	0.00	0.00
PI594449	Sichuan	China	VII	9	2	0	0	0	0.00	0.00
PI594458A	Sichuan	China	VII	5	2	0	0	0	0.00	0.00
PI594753A	Guangxi	China	VII	8	2	0	0	0	0.00	0.00
PI603537C	Shaanxi	China	VIII	8	2	0	0	0	0.00	0.00
PI603540A	Shaanxi	China	VII	10	2	0	0	0	0.00	0.00
PI603630	Hubei	China	VII	10	2	0	0	0	0.00	0.00
PI603722	Sichuan	China	VIII	9	2	0	0	0	0.00	0.00
PI603737B	Sichuan	China	VIII	9	2	0	0	0	0.00	0.00
PI458517	Shandong	China	III	3	2	0	0	0	0.00	0.00
PI458521	Jilin	China	III	9	2	0	0	0	0.00	0.00
PI468385	Jilin	China	III	9	2	0	0	0	0.00	0.00
PI479740	Jilin	China	III	11	2	0	0	0	0.00	0.00
PI567644	Henan	China	III	10	2	0	0	0	0.13	>10
PI594471A	Sichuan	China	III	8	2	0	0	0	0.33	>10
PI603655	Hunan	China	III	11	2	0	0	0	0.17	0.00
PI123590	Hebei	China	V	1	2	0	0	0	0.17	10.00
PI518291B	Liaoning	China	V	6	2	0	0	0	0.00	0.00
PI567233	Sichuan	China	V	10	2	0	0	0	0.00	0.00

Table 3.3. (cont.)

acid	Province	Country	MG	Plant Count	Chlorosis Index	Effective Nodules	Nodule Number	Nodule Weights	Average Number Plant^{-1}	Average Weight nodule^{-1}
PI588007A	Sichuan	China	V	6	2	0	0	0	0	0
PI594480A	Sichuan	China	V	7	2	0	0	0	0	0
PI597473	Hubei	China	V	8	2	0	0	0	0	0
PI603573B	Shanxi	China	V	7	2	0	0	0	0	0
PI603714	Sichuan	China	V	7	2	0	0	0	0	0
PI603720	Sichuan	China	V	6	2	0	0	0	0	0
PI183929	Meghalaya	India	VII	1	2	0	0	0	0	0
PI346308	unknown	India	IV	11	2	0	0	0	0	0
PI567041D	East Java	Indonesia	IX	5	2	0	0	0	0	0
PI567061	unknown	Indonesia	VIII	9	2	0	0	0	0	0
PI567081	East Java	Indonesia	VIII	3	2	0	0	0	0	0
PI200538	Shikoku	Japan	VIII	4	2	0	0	0	0	0
PI224269	Hyogo	Japan	VII	4	2	0	0	0	0	0
PI416826A	unknown	Japan	VIII	5	2	0	0	0	0	0
PI417126	Kyushu and Okinawa	Japan	VIII	6	2	0	0	0	0	0
PI594172C	Kumamoto	Japan	VIII	9	2	0	0	0	0	0
PI205087	unknown	Japan	III	10	2	0	0	0	0	0
PI227212	Shizuoka	Japan	III	7	2	0	0	0	0	0
PI261466	Kyushu	Japan	III	4	2	0	0	0	0	0
PI416902	Tohoku	Japan	III	10	2	0	0	0	0	0
PI507226A	Tohoku	Japan	III	4	2	0	0	0	0	0
PI548442	unknown	Taiwan	VIII	6	2	0	0	0	0	0
WILLIAMS 82	Illinois	United States	III	7	2	0	0	0	0	0
WILLIAMS 82	Illinois	United States	III	6	2	0	0	0	0	0
PI578458	An Giang	Vietnam	IX	2	2	0	0	0	0	0
PI605793	Cao bang	Vietnam	VI	5	2	0	0	0	0	0

Table 3.3. (cont.)

acid	Province	Country	MG	Plant Count	Chlorosis Index	Effective Nodules	Nodule Number	Nodule Weights	Average Number Plant^{-1}	Average Weight nodule^{-1}
PI606390B	(north)	Vietnam	VIII	3	2	0	0	0	0.00	0.00
PI324067	unknown	Zimbabwe	VII	7	2	0	0	0	0.00	0.00
PI324068	unknown	Zimbabwe	VIII	8	2	0	0	0	0.00	0.00
TGX 1908-8F				4	2	0	0	0	0.00	0.00
PI416868A	Kinki	Japan	III	7	1	0	110	50	15.71	0.45
PI567397	Shaanxi	China	V	10	1	1	48	100	4.80	2.08
PI179935	Himachal Pradesh	India	VII	4	1	0	47	70	11.75	1.49
PI605787D	Cao bang	Vietnam	VIII	6	1	1	39	160	6.50	4.10
PI587744	Hubei	China	V	5	1	1	14	50	2.80	3.57
PI060273	Zhejiang	China	V	8	1	1	10	90	1.25	9.00
PI605906	Hoa binh	Vietnam	VIII	10	1	1	10	30	1.00	3.00
PI518283	unknown	Taiwan	II	10	1	1	8	20	0.80	2.50
PI578440	(north)	Vietnam	IV	9	1	1	7	10	0.78	1.43
PI476880	(north)	Vietnam	IV	8	1	1	6	40	0.75	6.67
PI594511C	Sichuan	China	VIII	8	1	1	4	10	0.50	2.50
PI506887	Kanto	Japan	III	10	1	1	4	>10	0.40	>10
PI381677	unknown	Uganda	VI	3	1	1	2	10	0.67	5.00
PI605757	Lang son	Vietnam	VIII	4	1	1	1	10	0.25	10.00
PI567295	Gansu	China	VIII	11	1	1	0	0	0.00	0.00
PI594651	Guizhou	China	V	8	1	0	0	0	0.00	0.00
PI086452	Akita	Japan	III	9	1	0	0	0	0.00	0.00
PI506800B	Tohoku	Japan	III	3	1	0	0	0	0.00	0.00
PI476904	(north)	Vietnam	VII	1	1	0	0	0	0.00	0.00
PI476911	(north)	Vietnam	II	12	1	0	0	0	0.00	0.00
PI247678	Haut-Zaire	Zaire	VIII	9	1	0	0	0	15.71	0.45
PI587966A	Sichuan	China	VIII	6	1	0	0	0	4.80	2.08

Table 3.3. (cont.)

acid	Province	Country	MG	Plant Count	Chlorosis Index	Effective Nodules	Nodule Number	Nodule Weights	Average Number Plant^{-1}	Average Weight nodule^{-1}
PI588023A	Sichuan	China	VII	8	1	0	0	0	0	0
PI594502	Sichuan	China	VII	7	1	0	0	0	0	0
PI060296	Zhejiang	China	V	5	1	0	0	0	0	0
PI587975	Sichuan	China	V	6	1	0	0	0	0	0
PI587986B	Sichuan	China	V	7	1	0	0	0	0	0
PI594650B	Guizhou	China	V	8	1	0	0	0	0	0
PI486331	Maharashtra	India	IX	7	1	0	0	0	0	0
PI441352	Java	Indonesia	VIII	11	1	0	0	0	0	0
PI471899	Java	Indonesia	III	12	1	0	0	0	0	0
PI567087A	East Java	Indonesia	VIII	2	1	0	0	0	0	0
PI567089A	East Java	Indonesia	VIII	2	1	0	0	0	0	0
PI567130A	East Java	Indonesia	IX	6	1	0	0	0	0	0
PI229321	Kanto	Japan	VII	5	1	0	0	0	0	0
PI506528	Tohoku	Japan	III	10	1	0	0	0	0	0
PI210179	unknown	Taiwan	V	9	1	0	0	0	0	0
PI417569	unknown	Taiwan	VIII	10	1	0	0	0	0	0
PI578459	(north)	Vietnam	VII	8	1	0	0	0	0	0
PI605865A	Lao cai	Vietnam	V	10	1	0	0	0	0	0
PI587900C	Zhejiang	China	VIII	0	0	0	0	0	0	0
PI391597	Shaanxi	China	V	0	0	0	0	0	0	0
PI407759	Shanghai	China	V	0	0	0	0	0	0	0
PI549024	Liaoning	China	V	0	0	0	0	0	0	0
PI567269D	Guangdong	China	V	0	0	0	0	0	0	0
PI594776	Yunnan	China	V	0	0	0	0	0	0	0
PI438424	unknown	India	IV	0	0	0	0	0	0	0
PI438425	unknown	India	V	0	0	0	0	0	0	0

Table 3.3. (cont.)

acid	Province	Country	MG	Plant Count	Chlorosis Index	Effective Nodules	Nodule Number	Nodule Weights	Average Number Plant^{-1}	Average Weight nodule^{-1}
PI567122D	East Java	Indonesia	IX	0	0	0	0	0	0	0
PI567147C	Bali	Indonesia	IX	0	0	0	0	0	0	0
PI227219	Aichi	Japan	VII	0	0	0	0	0	0	0
PI417290	Shikoku	Japan	VIII	0	0	0	0	0	0	0
PI417442	Kanto and Tosan	Japan	VII	0	0	0	0	0	0	0
PI423908	Nagano	Japan	VII	0	0	0	0	0	0	0
PI506556	Kanto	Japan	VII	0	0	0	0	0	0	0
PI506579	Kanto	Japan	VIII	0	0	0	0	0	0	0
PI159096	North West	South Africa	VII	0	0	0	0	0	0	0
PI476914	(north)	Vietnam	IV	0	0	0	0	0	0	0
PI578452	Can Tho	Vietnam	VIII	0	0	0	0	0	0	0
PI578455A	Dong Nai	Vietnam	VIII	0	0	0	0	0	0	0
TGX 1485-1D				0	0	0	0	0	0	0
TGX 1740-2F				0	0	0	0	0	0	0
TGX 1835-10E				0	0	0	0	0	0	0
TGX 1987-10F				0	0	0	0	0	0	0
TGX 1987-76F				0	0	0	0	0	0	0
TGX 1987-118F				0	0	0	0	0	0	0
TGX1987-129F				0	0	0	0	0	0	0
TGX 1988-5F				0	0	0	0	0	0	0
PI085009-1	Saitama	Japan	III	4	0	0	0	0	0	0

Literature Cited

Giller, K.E., F. Javaheri, B. Mwakalombe, P. Davis, and S. Mpepereki,. 1998. Soybeans and Sustainable Agriculture: 'Promiscuous' soyabeans in Southern Africa. Biological Nitrogen Fixation for the 21st Century Current Plant Science and Biotechnology in Agriculture. 625-626. doi:10.1007/978-94-011-5159-7_388

Gwata, E.T., D.S. Wofford, P.L. Pfahler, and K.J. Boote. 2004. Genetics of promiscuous nodulation in soybean: Nodule dry weight and leaf color score. J. of Heredity. 95:154-157. doi:10.1093/jhered/esh017

Gwata, E. T., D.S. Wofford, K.J. Boote, A.R. Blount, and P.L. Pfahler. 2005. Inheritance of promiscuous nodulation in soybean. Crop Sci. 45:635. doi:10.2135/cropsci2005.0635

Imsande, J. and E.J. Ralston. 1981. Hydroponic growth and the nondestructive assay for dinitrogen fixation. Plant Physiol. 68:1380-1384.

Keyser, H.H., and F. Li. 1992. Potential for increasing biological nitrogen fixation in soybean. Biological Nitrogen Fixation for Sustainable Agriculture. 119-135. doi:10.1007/978-94-017-0910-1_7

Kueneman, E.A., W.R. Root, K.E. Dashiell, and J. Hohenberg. 1984. Breeding soybeans for the tropics capable of nodulating effectively with indigenous Rhizobium spp. Breeding Legumes for Enhanced Symbiotic Nitrogen Fixation. 115-124. doi:10.1007/978-94-009 5077-1_10

Pulver, E.L., E.A. Kueneman, and V. Ranga-Rao. 1985. Identification of promiscuous nodulating soybean efficient in N2 fixation. Crop Sci. 25:660-663. doi:10.2135/cropsci1985.0011183x002500040019x

Sanginga, N., R. Abaidoo, K. Dashiell, R.J. Carsky, and A. Okogun. 1996. Persistence and

effectiveness of rhizobia nodulating promiscuous soybeans in moist savanna zones of Nigeria. Applied Soil Ecology. 3:215-224.

Sanginga, N., J. Okogun, B. Vanlauw, and K. Dashiell. 2002. The contribution of nitrogen by promiscuous soybeans to maize based cropping the moist savanna of Nigeria. Plant Soil. 241:223-231. doi:10.1023/A:1016192514568

Sinclair, T.R., H. Marrou, A. Soltani, V. Vadez, and K.C. Chandolu. 2014. Soybean production potential in Africa. Global Food Security. 3:31-40. doi:10.1016/j.gfs.2013.12.001